



Published in final edited form as:

Sci Transl Med. 2016 May 25; 8(340): 340ra72. doi:10.1126/scitranslmed.aaf1059.

## Amyloid- $\beta$ Peptide Protects Against Microbial Infection In Mouse and Worm Models of Alzheimer's Disease

Deepak Kumar Vijaya Kumar<sup>1,†</sup>, Se Hoon Choi<sup>1,†</sup>, Kevin J. Washicosky<sup>1,†</sup>, William A. Eimer<sup>1</sup>, Stephanie Tucker<sup>1</sup>, Jessica Ghofrani<sup>1</sup>, Aaron Lefkowitz<sup>1</sup>, Gawain McColl<sup>2</sup>, Lee E. Goldstein<sup>3</sup>, Rudolph E. Tanzi<sup>\*1</sup>, and Robert D. Moir<sup>\*1</sup>

<sup>1</sup>Genetics and Aging Research Unit, MassGeneral Institute for Neurodegenerative Disease, Department of Neurology, Massachusetts General Hospital and Harvard Medical School, Charlestown, Massachusetts, United States of America.

<sup>2</sup>The Florey Institute of Neuroscience and Mental Health, University of Melbourne, Victoria, Australia.

<sup>3</sup>Department of Psychiatry, Boston University, Boston, Massachusetts, United States of America.

### Abstract

The amyloid- $\beta$  peptide ( $A\beta$ ) is a key protein in Alzheimer's disease (AD) pathology. We previously reported in vitro evidence suggesting that  $A\beta$  is an antimicrobial peptide. We present in vivo data showing  $A\beta$  expression protects against fungal and bacterial infections in mouse, nematode, and cell culture models of AD. We show that  $A\beta$  oligomerization, a behavior traditionally viewed as intrinsically pathological, may be necessary for the antimicrobial activities of the peptide. Collectively, our data are consistent with a model in which soluble  $A\beta$  oligomers

\*Correspondence to: Robert Moir, Ph.D. Genetics and Aging Research Unit, Massachusetts General Hospital, Building 114 16th Street Charlestown, MA 02129, USA Tel (617) 726 3746; Fax (617) 724 1823, moir@helix.mgh.harvard.edu And Rudolph E. Tanzi, Ph.D., Director, Genetics and Aging Research Unit, Massachusetts General Hospital, Building 114 16th Street Charlestown, MA 02129, USA Tel (617) 726 6845; Fax (617) 724 1823, Tanzi@helix.mgh.harvard.edu.

†Authors contributed equally to this study.

### Supplementary Materials

Table S1: Figure micrographs are representative of data from multiple repeat experiments and image fields.

Fig. S1:  $A\beta$  deposition and inflammation in 5XFAD mice prior to infection and criteria used for assessing clinical performance following infection.

Fig. S2:  $A\beta_{42}$  localizes to gut and muscle in GMC101 nematodes.

Fig. S3:  $A\beta$  expression protects GMC101 nematodes and CHO-CAB cells against *S. Typhimurium*.

Fig. S4: Confirmation of increased *Candida* resistance among transformed host cells using three independent assays.

Fig. S5: Transformed cell lines generate  $A\beta$  oligomers at levels found in the soluble fraction of human brain.

Fig. S6: Transformed H4- $A\beta_{40}$  and CHO-CAB host cells resist *Candida* colonization and agglutinate yeast.

Fig. S7: Birefringence of Congo red stained yeast aggregates from H4- $A\beta_{42}$  media.

Fig. S8: Anti- $A\beta$  antibodies do not label CL2122 tissues or yeast.

Fig. S9:  $\beta$ -amyloid co-localizes with *S. Typhimurium* cells in 5XFAD brain.

Fig. S10: Model for antimicrobial activities of soluble  $A\beta$  oligomers.

Video S1: Z-section projection of 5XFAD mouse brain showing  $\beta$ -amyloid entrapment of *S. Typhimurium* cells.

**Author Contributions:** D.K.V.K., S.H.C., K.J.W., R.D.M., and R.E.T were responsible for experimental design and data interpretation. R.D.M. and R.E.T. were responsible for manuscript preparation with assistance from D.K.V.K., S.H.C., and K.J.W. L.E.G. and G.M. contributed to experimental design, data interpretation and developed the nematode models. W.A.E., S.T., J.G., and A.L. conducted experiments.

The contributions of D.K.V.K., S.H.C., and K.J.W. overlapped extensively and include collaborations on the studies in vitro assays, cell culture, nematode, and mouse experiments. The three first authors contributed equally to this study

**Competing interests:** The authors have no competing interests pertaining to this work.

bind to microbial cell wall carbohydrates via a heparin-binding domain. Developing protofibrils inhibit pathogen adhesion to host cells. Propagating  $\beta$ -amyloid fibrils mediate agglutination and final entrapment of microbes.. Consistent with our model, *Salmonella* Typhimurium bacteria infections of the brains of transgenic 5XFAD mice resulted in rapid seeding and accelerated  $\beta$ -amyloid deposition, which closely co-localized with the invading bacteria. Our findings raise the intriguing possibility that  $\beta$ -amyloid may play a protective role in innate immunity and infectious or sterile inflammatory stimuli may drive amyloidosis. These data suggest a dual protective/damaging role for  $A\beta$ , as has been described for other antimicrobial peptides.

## Introduction

Neurodegeneration in Alzheimer's disease (AD) is mediated by soluble oligomeric intermediates generated during fibrillization of the amyloid- $\beta$  protein ( $A\beta$ ) (1). Overwhelming evidence supports  $A\beta$ 's pivotal role in AD. However, despite remarkably high sequence conservation across diverse species (humans share  $A\beta_{42}$  sequences with coelacanths, a 400 million year old fish taxon) (2) and extensive data showing broad activity spectra for  $A\beta$ , the peptide has traditionally been characterized as a functionless catabolic byproduct. Activities identified for  $A\beta$  in vivo are most often described as stochastic pathological behaviors. Oligomerization in particular is viewed as a pathogenic pathway and  $A\beta$  oligomers are assumed to be intrinsically abnormal. Scant consideration has been given to possible physiological roles for  $A\beta$ .

Members of the evolutionarily ancient family of proteins, collectively known as antimicrobial peptides (AMPs), share many of  $A\beta$ 's purportedly abnormal activities, including oligomerization and fibrillization (3, 4). For AMPs, these activities mediate key protective roles in innate immunity. AMPs are the first-line of defense against pathogens and act as potent broad-spectrum antibiotics and immunomodulators that target bacteria, mycobacteria, enveloped viruses, fungi, and protozoans, and in some cases, transformed or cancerous host cells (5). AMPs are widely expressed and are abundant in brain and other immunoprivileged tissues where actions of the adaptive immune system are constrained. Although AMPs are normally protective, AMP dysregulation can lead to host cell toxicity, chronic inflammation, and degenerative pathologies (6–8). Particularly germane to  $A\beta$ 's role in AD, AMPs are deposited as amyloid in several disorders (3, 4, 9) including senile seminal vesicle amyloid and isolated atrial amyloidosis, two of the most common human amyloidopathies. Consistent with identity as an AMP, we recently reported that synthetic  $A\beta$  exhibits potent in vitro antimicrobial activity towards eight common and clinically relevant microbial pathogens (3). Furthermore, whole brain homogenates from AD patients show  $A\beta$ -mediated activity against *Candida albicans*. More recently, synthetic  $A\beta$  has been shown to protect cultured cells from influenza A virus (10) and herpes simplex virus (11). However, the biological relevance of protective in vitro  $A\beta$  activities requires validation in vivo. In this study we extend our original findings and show that  $A\beta$  expression inhibits infection in a transgenic mouse model of AD (5XFAD), in the nematode *Caenorhabditis elegans* and in cultured mammalian cell models. Mice lacking the amyloid precursor protein (APP) that have low  $A\beta$  expression also show a trend towards attenuated survival after bacterial infection. Most surprisingly, oligomerization and fibrillization appear to mediate  $A\beta$ 's

protective activity, and cerebral infection with microbial cells seeds and dramatically accelerates  $\beta$ -amyloid deposition in 5XFAD mice and transgenic *C. elegans*.

## Results

A $\beta$ -mediated protection was characterized in mice, *C. elegans*, and cell culture models of infection. *Salmonella enterica* serotype typhimurium (*S. typhimurium*) was used as an infecting agent in mouse models. Nematode and cultured cell experiments used pathogenic (hyphal) *Candida albicans* (*Candida*) and *S. typhimurium*.

### A $\beta$ protects against meningitis in genetically modified mice

We first used genetically modified mice to test for protective effects of elevated A $\beta$  expression and attenuated resistance with decreased peptide. Four-week old 5XFAD transgenic mice constitutively express human A $\beta$  in the brain at high levels but lack the  $\beta$ -amyloid deposits and features of neuroinflammation found in older animals (12). APP knockout (APP-KO) mice lack the precursor protein required for murine A $\beta$  generation (13). One-month old 5XFAD mice ( $n = 12$ ), APP-KO mice ( $n = 15$ ), and wildtype (WT) littermates ( $n = 11$  and  $15$ , respectively) received a single intra-cerebral injection of 65,000 colony-forming units (CFU) of *S. typhimurium*. Clinical progression to the moribund state was followed according to established grading criteria for mouse encephalomyelitis (fig. S1A). Survival of A $\beta$ -expressing 5XFAD mice was significantly increased compared to non-transgenic littermates ( $P = 0.009$ ) (Fig. 1A). Consistent with increased resistance to infection, 5XFAD mice also ranked significantly higher in clinical tests grading mouse encephalomyelitis progression ( $P < 0.0001$ ). 5XFAD mice also showed reduced weight loss ( $P = 0.0008$ ) and lower cerebral *S. typhimurium* loads ( $P = 0.03$ ) compared to WT controls (Figs. 1B to D). Consistent with immunodeficiency associated with low A $\beta$ , APP-KO mice showed a trend ( $P = 0.10$ ) towards increased mortality after infection (Fig. 1E). Control injections using heat-killed bacteria did not lead to clinical decline or death in 5XFAD and WT mice (Fig. 1F), consistent with mouse mortality being mediated by *S. typhimurium* infection. Next, we confirmed high amounts of soluble A $\beta$  and low amounts of insoluble A $\beta$  in four-week old 5XFAD mouse brain using formic acid extraction and anti- $\beta$ -amyloid ELISA assay (fig. S1B). To confirm inflammation did not immunologically prime and protect 5XFAD mice against infection, we compared the immune profiles in one-month old transgenic and WT mouse brain. Consistent with previous reports showing an absence of immune activation (12), there was no significant increase in GFAP<sup>+</sup> astrocytes, Iba1<sup>+</sup> microglia, and the amounts of ten cytokines in four-week old 5XFAD mice compared to WT littermates (figs. S1C to E).

### A $\beta$ increases survival of transgenic *C. elegans* infected with *Candida*

To further explore the ability of A $\beta$  to afford protection against infection, we next tested transgenic *C. elegans* for resistance to *Candida*. Our nematode infection model uses two previously described *C. elegans* transgenic strains: GMC101 that expresses the 1-42 residue human A $\beta$  isoform (A $\beta$ 42) (14) and CL2122, a control strain that expresses intestinal GFP (*mtl-2:gfp*) marker (as does GMC101) but does not express A $\beta$ . Adult GMC101 nematodes ultimately develop age-progressive paralysis and  $\beta$ -amyloid deposition in the body wall

muscle. For our experiments, developmentally synchronized L4 larvae were infected five days prior to the onset of paralysis. A $\beta$  expression is driven by the *unc-54* promoter (which encodes a myosin heavy chain), active in body wall muscle (14) as well as in other tissues, including muscle cells of the gastrointestinal (GI) track (15). Amyloidogenic peptides under the *unc-54* promoter have also been shown to translocate via vesicular transport to the gut of transgenic worms and A $\beta$  has been proposed as a likely candidate for translocation via this mechanism (16). Immunohistological analysis of adult GMC101 using three different anti-A $\beta$  antibodies confirmed A $\beta$  localization in the body wall muscle and the gut lumen (fig. S2A and B). Anti-A $\beta$  antibodies did not label negative control strain CL2122 intestine or body wall cells. In addition, excreta from healthy GMC101 but not CL2122 worms were positive for anti-A $\beta$  signal by immunoblot (Fig. S2C). While an origin for gut A $\beta$  remains unclear, strong empirical evidence supports the localization of A $\beta$  peptides in the intestinal lumen of GMC101 nematodes. Thus, transgenic GMC101 nematodes appear to be suitable models for testing A $\beta$ -mediated protective activities against intestinal pathogens.

*C. albicans* (ATCC 90028) is an A $\beta$ -sensitive microbial organism (3) and a well-characterized *C. elegans* intestinal pathogen that causes distention, penetrative filamentation, and death among wild-type nematodes 2 days after ingestion. Links between fungal brain infections and AD pathology have also recently emerged, including for *C. albicans* (17) and closely related *Candida glabrata* (18). We compared survival of control CL2122 ( $n = 56$ ) and GMC101 ( $n = 59$ ) nematodes after incubation (2 hrs, 25° C) on *C. albicans* lawns. Consistent with A $\beta$ -mediated protection, GMC101 nematodes infected with *C. albicans* showed significantly ( $P < 0.00001$ ) reduced mortality as compared to control CL2122 worms that did not express A $\beta$  (Fig. 2A). Consistent with mouse data, A $\beta$  expressing nematodes were also protected from the *C. elegans* intestinal pathogen *S. typhimurium*, with GMC101 worms showing statistically significant ( $P = 0.0005$ ) increased survival compared to CL2122 controls following infection with the bacterium (fig. S3A).

### The antimicrobial activities of A $\beta$ protects cell in culture

To address the mechanism of protection, we next tested the ability of A $\beta$  to protect cell monolayers from infection using transformed cultured human brain neuroglioma (H4) and Chinese hamster ovary (CHO) cells. H4 lines include stably transformed H4-A $\beta$ 40 and H4-A $\beta$ 42 cells that selectively secrete the 1–40 residue A $\beta$  isoform (A $\beta$ 40) or A $\beta$ 42 isoform, respectively (19). Processing of a BRI-A $\beta$  fusion protein expressed by transformed H4 cells led to constitutive high-level expression and secretion of the encoded A $\beta$  protein. For double transfected CHO cells, overexpression of APP and the APP-processing protease  $\beta$ -secretase (CHO-CAB) leads to APP cleavage and the generation of multiple A $\beta$  isoforms (20). Non-transformed H4 (H4-N) and CHO (CHO-N) cells were used as control cell lines. *C. albicans* has been extensively characterized in cell culture infection models and was used in our experiments as an infectious agent.

We first compared non-transformed and transformed host cells for survival following infection with *C. albicans*. Host cells were pre-labeled with BrdU. After infection host cell viability was determined by assaying for anti-BrdU immunofluorescence signal. Consistent with findings for 5XFAD mice and GMC101 nematodes, survival 28 hours post-infection

was significantly increased for A $\beta$  overexpressing H4-A $\beta$ 40 ( $P=0.002$ ) and H4-A $\beta$ 42 ( $P=0.001$ ) transformed cell lines compared to control H4-N cells with rank order H4-A $\beta$ 42 > H4-A $\beta$ 40 > H4-N (Fig. 2B). Survival of transformed CHO-CAB cells was also significantly higher ( $P=0.004$ ) than control CHO-N cell lines. Additional independent assays of host cell viability (figs. S4A and B) were performed to confirm increased resistance of transformed H4-A $\beta$ 42 cells to *C. albicans* infection. Attenuated *C. albicans* load for H4-A $\beta$ 42 cells was also independently confirmed by comparing wells for yeast CFUs (fig. S4C)

Whereas the amount of A $\beta$  in conditioned cell culture media (figs. S5A and B) fell within the physiological ranges reported for human cerebrospinal fluid (CSF) (2–20 ng/ml) (21), concentrations were two orders of magnitude ( $\log_{10}$ ) lower than the minimal inhibitory concentration (MIC) for fungicidal activities in microdilution MIC assays (3). We have previously reported that A $\beta$ 's antimicrobial activities show close parallels with those of LL-37 (3), an archetypal human AMP that remains protective at sub-fungicidal concentrations (22). Two linked, yet distinct activities mediate LL-37's protective anti-*Candida* actions at low peptide concentrations (22). The first is disruption of *C. albicans* adhesion to host cells. Host cell attachment is a prerequisite step for infection by many pathogens, including *C. albicans*. The second is agglutination of the resulting unattached yeast cells. Agglutination limits microbial access to host cells and also generates high local AMP concentrations within peptide/microbe aggregates. Accordingly, we next tested A $\beta$  for adhesion inhibition and agglutination activities using the cell culture infection model. Hyphal *C. albicans* was incubated (2 hrs, 37 °C) in preconditioned media with transformed or non-transformed cell cultures prepared in slide chambers. Microscopic examination revealed fewer *C. albicans* attached to transformed A $\beta$ -expressing cells compared to non-transformed) monolayers (Fig. 2C and fig. S6A). To confirm these data, *C. albicans*-cell culture incubation experiments were repeated in 96-well microtiter plates and the *Candida* load in wells was assayed immunochemically using anti-*Candida* antibodies. Data confirmed visual observations with statistically significant attenuation of *C. albicans* adhesion to transformed H4-A $\beta$ 42 ( $P=0.001$ ), H4-A $\beta$ 40 ( $P=0.001$ ) and CHO-CAB ( $P=0.004$ ) cells compared to naive control lines (Fig. 2D). Additionally, after overnight incubation dramatic microbial agglutination was observed in wells containing transformed, but not non-transformed, host cells (Fig. 2E and fig. S6B). Images of wells were analyzed for yeast aggregation. *Candida* aggregation was significantly elevated in transformed H4-A $\beta$ 42 ( $P=0.00004$ ), H4-A $\beta$ 40 ( $P=0.0003$ ), and CHO-CAB ( $P=0.002$ ) samples compared to naive controls (Fig. 2F). For H4 cell lines, adhesion inhibition and agglutination activities were consistent with host viability data with rank orders H4-A $\beta$ 42 > H4-A $\beta$ 40 > H4-N cell lines.

We next characterized cell-free conditioned culture media for A $\beta$ -mediated adhesion inhibition and agglutinating activities. Yeast adhesion and agglutination were assayed in 96-well plates using the methods of Tsai *et al.* (22). Briefly, hyphal *C. albicans* were incubated (2 hrs, 37 °C) with conditioned media samples in the absence of host cells. After washing, yeast adhering to abiotic well surfaces were stained with Calcofluor White and well fluorescence measured. Well images were analyzed for yeast aggregation after overnight incubation. Immunodepletion with anti-A $\beta$  antibodies significantly attenuated H4-A $\beta$ 42, H4-A $\beta$ 40, and CHO-CAB media adhesion inhibition ( $P=0.009$ ,  $P=0.001$ , and  $P=0.004$ , respectively) and agglutination ( $P=0.001$ ,  $P=0.0005$ , and  $P=0.004$ , respectively) activities

against *C. albicans* (Figs. 3A–B). Analysis confirmed that anti-A $\beta$ -immunodepletion removed > 95% of the A $\beta$  from samples used in experiments to confirm that the anti-*Candida* activities of transformed cell culture media were specific for A $\beta$  (Figs. S5A–B).

Consistent with yeast data, *S. typhimurium* were agglutinated in H4-A $\beta$ 42 conditioned media. (Fig. S3B). H4-A $\beta$ 42 cell cultures incubated with *S. Typhimurium* also have significantly ( $P= 0.036$ ) lower intracellular infection compared to non-transformed H4-N cells (Fig. S3C–D).

Serial dilution experiments showed that adhesion inhibition and agglutination activities were dose-dependent for both synthetic and cell-derived A $\beta$  (Figs. 3C–D). However, synthetic A $\beta$  peptide preparations had lower specific activities compared to cell-derived material. Co-factors secreted by cultured cells were unlikely to account for the increased potency of cell-derived A $\beta$  since synthetic peptide incubations were performed in A $\beta$ 42-depleted conditioned media (H4-A $\beta$ 42-ID) from H4-A $\beta$ 42 cell cultures. Anti-A $\beta$  antibodies used to clear A $\beta$ 42 from H4-A $\beta$ 42 culture media prior to addition of synthetic peptides were specific for A $\beta$  and not likely to deplete species acting as co-factors. Oligomerization has been shown to modulate a range of A $\beta$  activities. Moreover, conditioned media from experimental cell lines has been reported to contain oligomeric A $\beta$  (23), whereas our synthetic peptide preparations were pre-treated to remove oligomer species. Synthetic peptide pre-treatments included fractionation by preparative size exclusion chromatography to remove species >6 kDa. Characterization experiments using analytical size exclusion chromatography confirmed that immediately prior to experimental inoculation with yeast, cell-derived material contained a polydisperse population of soluble A $\beta$  oligomers of between 8 and 50 kDa, whereas synthetic peptides remained overwhelmingly monomeric (Fig. S5C).

To test whether oligomerization modulates A $\beta$ 's AMP activity, we generated synthetic A $\beta$  oligomers and compared the antimicrobial activities of A $\beta$ 42 monomer, soluble oligomeric ADDLs (amyloid- $\beta$  derived diffusible oligomeric ligands) (24), and high-order protofibril (>600 kDa) preparations. Compared to monomeric peptide, ADDLs exhibited potentiated, and protofibrils attenuated, adhesion inhibition (Fig. 3E) and agglutination (Fig. 3F) activities. Our data are consistent with a central role for soluble A $\beta$  low-order (2–30 monomer units) oligomers in mediating the peptide's AMP activities. Consistent with such a role, soluble A $\beta$  is overwhelmingly oligomeric in vivo (25) and oligomers are key for the protective activities of a wide range of AMPs (26–29) including LL-37 (26, 30).

### Antimicrobial actions are mediated by heparin-binding activity of A $\beta$ oligomers

Binding of AMP peptides to microbial surfaces is a prerequisite step for adhesion inhibition and agglutination activities. LL-37 contains a XBBXB heparin-binding motif (where X is a hydrophobic or uncharged residue, and B is a basic residue) that mediates inhibition of host adhesion and agglutination activities by facilitating attachment of oligomeric species (26, 30) to microbial cell wall carbohydrates (22). A $\beta$  also contains a XBBXB heparin-binding motif between residues 12–17 (VHHQKL) (31). Competitive inhibition by soluble microbial sugars is a hallmark for AMPs with activities mediated by lectin-like carbohydrate binding (22). Indeed, fungal and bacterial pathogens secrete specialized scavenging

exopolysaccharides that target the heparin-binding domains of AMPs as a counter-measure to defenses mounted by hosts. Soluble forms of mannan and glucan, the two most abundant carbohydrates in the yeast cell wall, have been shown to inhibit XBBXB-mediated binding of LL-37 to *Candida* (22, 32). We investigated if the adhesion inhibition and agglutination activities of A $\beta$  are similarly inhibited by soluble mannan and glucan. Live yeast cells were incubated in H4-A $\beta$ 40, H4-A $\beta$ 42, and CHO-CAB conditioned media in the presence or absence of mannan or glucan. Consistent with anti-*Candida* activity mediated by A $\beta$ 's heparin-binding domain, mannan and glucan significantly attenuated adhesion inhibition ( $P < 0.008$ ) and agglutination ( $P < 0.003$ ) activities of conditioned media from A $\beta$ -expressing transformed cells (Figs. 3G–H).

We further characterized A $\beta$ 's binding to *C. albicans* and *S. Typhimurium* using a new binding immunoassay. For this assay, samples were incubated in wells containing immobilized intact hyphal *Candida* or *S. Typhimurium* cells and bound A $\beta$  was detected immunochemically with an A $\beta$ 42-specific antibody. A $\beta$  binding to *Candida* and *S. Typhimurium* was concentration dependent (Figs. 3I and S3E). Consistent with binding mediated by A $\beta$ 's VHHQKL domain, anti-A $\beta$  signal from H4-A $\beta$ 42 media was significantly attenuated in the presence of glucan ( $P = 0.008$ ) or mannan ( $P = 0.004$ ) (Fig. 3J), consistent with inhibition of A $\beta$  yeast binding. Well anti-A $\beta$  signal was also significantly reduced ( $P = 0.006$ ) for anti-A $\beta$ -immunodepleted H4-A $\beta$ 42 media (negative control), which is consistent with assay specificity for A $\beta$ 42 binding. Consistent with findings for antimicrobial activities, cell-generated A $\beta$  oligomers show increased binding to immobilized yeast compared to synthetic monomeric peptide (Fig. 3I). Previous studies have shown that A $\beta$  oligomerization greatly increases carbohydrate-binding activity (31). Heparin-binding AMP oligomers also show potentiated carbohydrate binding compared to monomeric species (33). Overall, our findings are consistent with soluble A $\beta$  oligomers possessing an enhanced propensity to bind to cell walls, engendering greater adhesion inhibition and agglutination activities compared to monomeric synthetic peptide.

### A $\beta$ fibrillization mediates *Candida* agglutination

Binding by A $\beta$  of glycosaminoglycans found in brain induces the peptides fibrillization (34). A $\beta$ 's binding of cell wall and glycocalyx carbohydrates to microbial surfaces seem likely to also generate A $\beta$  fibrils. While viewed solely as a part of A $\beta$ 's pathophysiology, fibrillization among AMPs is a normal protective behavior that mediates antimicrobial activities, including microbial cell and viral agglutination (35) and bacterial membrane perturbation (3, 4). Most recently, studies have shown that the human AMP  $\alpha$ -defensin-6 (HD6) forms fibrils that entangle and trap microbial cells (36). Thus, we next investigated a possible role for A $\beta$  fibrillization in the peptides protective AMP activities. Analysis of early-stage (< 3 hrs post infection) *Candida* agglutination in H4-A $\beta$ 42 media using transmission electron microscopy (TEM) revealed clumped microbial cells entwined and linked by fibrils propagating from cell surfaces (Fig. 4A–D). *Candida albicans* lack flagella and are not reported to produce extended fibrillar structures. Moreover, the fibrillar structures on the yeast cell surface were labeled by anti-A $\beta$  immunogold nanoparticles (anti-A $\beta$ -Au). Anti-A $\beta$ -Au binding to fibrils was ablated by co-incubation with synthetic A $\beta$  peptide, consistent with A $\beta$ -specific labeling (Fig. 4D). TEM analysis of early stage *S. Typhimurium* agglutinates in H4-A $\beta$ 42

conditioned media confirmed that bacterial cells were also bound and linked by fibrils (Fig. S3F).

Epifluorescence micrographs of Thioflavin S stained late-stage (>12 hrs post infection) H4-A $\beta$ 42 yeast aggregates displayed the enhanced fluorescence and red shifts that mark the presence of amyloid fibrils (Fig. 5A). Enhanced fluorescence was not observed for negative control yeast agglutinates (Fig. 5A). Thioflavin S fluorescence within H4-A $\beta$ 42 yeast aggregates co-localized with the signal for anti-A $\beta$  immunoreactivity (Fig. 5B). Congo red stained H4-A $\beta$ 42 yeast aggregates also showed birefringence under polarized light, another marker for  $\beta$ -amyloid (Fig. S7). Scanning EM (SEM) micrographs of yeast aggregates from H4-A $\beta$ 42 media revealed an irregular material adhering to cell surfaces not present in *Candida* pellets prepared by centrifugation in A $\beta$ -free media (Fig. 5C). Analysis of the *Candida* cell surface by TEM revealed the adhering material to be filamentous and immunoreactive to anti-A $\beta$ -Au (Fig. 5D). Co-incubation of soluble synthetic A $\beta$ 40 peptide abolished anti-A $\beta$ -Au binding. Collectively, the data are consistent with microbial agglutination and entrapment mediated by A $\beta$  fibrillization in our cell culture infection model.

### **$\beta$ -amyloid mediated pathogen entrapment in the GMC101 nematode and 5XFAD mice**

We also investigated infection-associated A $\beta$  fibrillization in our nematode and mouse infection models. Consistent with A $\beta$  targeting and binding to yeast cells in our cell culture model, *Candida* in the gut of recently infected (2 hrs post ingestion) GMC101 nematodes were labeled by anti-A $\beta$ -Au nanoparticles (Fig. 6A). Yeast in the gut of the control CL2122 nematode were not labeled by anti-A $\beta$ -Au (Fig. S8A). A $\beta$  fibrillization in GMC101 worms is normally confined to the body wall muscle. However, compared to infection-free nematodes, GMC101 worms with late-stage *Candida* infection showed enhanced Thioflavin fluorescence in non-muscle tissue, including the gastrointestinal track (Fig. 6B). High resolution micrographs of yeast cells in the gastrointestinal track of GMC101 nematodes revealed clumped *Candida* embedded in material that showed enhanced fluorescence after Thioflavin staining (Fig. 6C) and was labeled by anti-A $\beta$  antibodies (Fig. 6D). Consistent with A $\beta$ -specific labeling, anti-A $\beta$  signal (Figs. S2B) and enhanced Thioflavin S fluorescence (Fig. S8B) were absent from uninfected or *Candida* infected negative control CL2122 nematodes that did not express A $\beta$ . Findings for *C. albicans* infected GMC101 nematodes were consistent with the agglutinating and entrapment roles of A $\beta$  fibrils observed in our cell culture infection models. Thus, A $\beta$  fibrillization on the surface of yeast cells infecting the gut of GMC101 nematodes may mediate the infection resistance observed for these worms.

Four-week old 5XFAD mouse brain is normally negative for  $\beta$ -amyloid deposits (12). However, Thioflavin S and anti-A $\beta$  staining of 5XFAD mouse brain revealed widespread  $\beta$ -amyloid deposition 48 hours after infection with *S. Typhimurium* (Fig. 7). Moreover, anti-*Salmonella* and  $\beta$ -amyloid signal colocalized in 5XFAD mouse brain suggesting bacterial cells may have induced A $\beta$  fibrillization. TEM analysis also revealed that bacterial cells were embedded in fibrous material labeled by anti-A $\beta$ -Au nanoparticles in 5XFAD but not wildtype mouse brain sections (Fig. S8). Video of Z-section projections rotating through



360° show that bacteria are not confined to the surface of A $\beta$  accretions but are embedded within the  $\beta$ -amyloid deposits (Video S1). Consistent with fibrillization driven by proliferation of *S. Typhimurium* cells,  $\beta$ -amyloid deposits were absent from sham-infected one-month old 5XFAD control mice injected with heat-killed bacteria. Thioflavin S staining and anti- $\beta$ -amyloid antibodies did not label mouse brain from negative control non-transgenic littermates (Fig. 7A).

## Discussion

Our findings are consistent with a potential protective role for A $\beta$  in vivo as an AMP. Expression of A $\beta$  was associated with increased host survival in cell culture, nematode, and mouse infection models (Figs. 1 and 2). Low A $\beta$  expression was associated with higher mortality after infection of APP-KO mice. Our data are consistent with a protective role for A $\beta$  in innate immunity that employs a classic AMP mechanism characterized by reduced microbial adhesion to host cells and, agglutination and entrapment of microbes by  $\beta$ -amyloid fibrils. Moreover, well-characterized A $\beta$  activities mediate the peptides antimicrobial actions. However, these same properties, e.g. oligomerization, fibrillization, and carbohydrate binding, are also linked to A $\beta$ 's pathophysiology. While a protective/damaging duality is a new proposition for A $\beta$ 's activities, this is not the case for classical AMPs. For example, LL-37 offers a germane model for the potential pathological consequences of normally protective AMP actions. LL-37 is essential for normal immune function, and low expression leads to lethal infections (37). However, at elevated concentrations, LL-37 is cytotoxic to host cells, particularly smooth muscle cells (38). The cytotoxic and proinflammatory activities of LL-37 are implicated in the pathogenesis of several major late-life diseases, including rheumatoid arthritis, lupus erythematosus, and atherosclerosis (39). Thus, a normally protective A $\beta$  activity spectra that, when dysregulated also leads to AD pathology, is consistent with the actions of classical human AMPs.

Adhesion blocking and agglutination activities are distinct from AMP microbicidal activities, which typically require micromolar concentrations of peptide and involve different mechanisms (22). The adhesion inhibition and agglutination activities we observed in vitro for cell-derived A $\beta$  (Fig. 3) fall within physiological concentration ranges reported for normal human cerebrospinal fluid (CSF) (1 to 5 ng/ml). Consistent with a normal in vivo protective role the highest cerebral concentrations of A $\beta$  are in the leptomeninges (10 to 50 ng/ml) (40), the brain's first line of defense against infection and a tissue enriched for LL-37 and other innate immune proteins (41). The high specific activity observed for cell-derived material is consistent with our previous finding that A $\beta$  in human brain extracts is a potent anti-*Candida* agent (3). Classical AMP expression can be either constitutive or inducible (5). In our transgenic mouse, nematode, and cultured cell models, constitutive expression of A $\beta$  is maintained artificially. As such, our models are not suitable for testing whether infection normally results in A $\beta$  upregulation. However, data from other investigators suggest that A $\beta$  may be an inducible AMP. Host cell exposure to HSV-1 (42), HIV1 (42), spirochetes (43), or chlamydia (44, 45) increase A $\beta$  expression.

In in vitro assays, cell-derived and synthetic A $\beta$  oligomers were more potent against *Candida* than were monomeric forms (Figs. 3C to F and fig. S5C). The specific activities of

synthetic ADDLs, while higher than non-oligomerized peptide, remain lower than cell-derived A $\beta$  species. Peptide posttranslational modifications may enhance the AMP activity of cell-derived A $\beta$  oligomers. However, oligomer conformation is also likely to play a key role. Neurotoxicity has been shown to be highly dependent on the arrangement of A $\beta$  peptides within oligomeric assemblies. Oligomer morphology may also modulate A $\beta$ 's protective antimicrobial activities. Protocols for preparing ADDLs and other synthetic A $\beta$  assemblies are optimized for oligomer populations with neurotoxic, not antimicrobial, activities. Future protocols optimized for enhanced AMP activities may generate soluble synthetic A $\beta$  oligomers with potencies that approach that of cell-derived material.

A $\beta$  pathophysiology is thought to arise from an abnormal propensity to generate soluble oligomers. However, oligomerization is not a pathogenic behavior for AMPs and it plays a key role in normal protective activities across this diverse group of proteins, including microbe agglutination and entrapment (35), the targeting (26, 30) and disruption of microbial cell membranes (4, 46), resistance to bacterial proteases (26, 27, 46), and expanding the molecular diversity and protective functions of AMP families without commensurate genome expansion (28, 29). Our data and the widespread involvement of oligomerization in the protective actions of AMPs suggest that the brain's pool of soluble A $\beta$  may normally include physiologically functional oligomeric species that mediate protective antimicrobial activities. The intrinsic polymorphic stoichiometry of A $\beta$  oligomers may also play a protective physiological role in that the A $\beta$  oligomers were more potent against *Candida* than monomeric forms. As has been shown with classical AMPs, diverse polymorphic oligomer pools target a broader spectrum of pathogens and are more resistant to AMP-targeting microbial proteases than are homogenous peptide populations.

The lectin activity of A $\beta$  oligomers is thought to promote brain amyloidosis (34). Studies to date have focused on accelerated A $\beta$  fibrillization induced by binding of endogenous brain proteoglycans and glycosaminoglycans. However, our findings suggest that A $\beta$  oligomers also bind to microbial carbohydrates with high affinity (figs. 3G to J). Carbohydrate-binding activity among AMPs is widespread and normally protective, playing a key role in helping peptides to recognize and bind to microbial pathogens (22). Heparin-binding AMPs have high affinities for the unique microbial carbohydrates found in cell walls but also bind to host glycosaminoglycans (47). Consistent with our findings for A $\beta$ , binding of classical AMPs to microbial carbohydrate can lead to rapid peptide fibrillization and amyloid-mediated antimicrobial activities (48). Dysregulated carbohydrate-binding by A $\beta$  may play a role in AD amyloidogenesis. However, a normal role as an AMP would suggest that polymeric microbial cell surface carbohydrates may be the normal *in vivo* target for the heparin-binding activity of oligomeric A $\beta$  species.

Long recognized as a key defensive strategy among lower organisms, AMP-mediated microbial agglutination is also emerging as an important part of human immunity (49). AMP fibrillization appears to play a central role in this important protective activity (35). Most recently, *in vivo* fibrillization of HD6 has been shown to mediate not only agglutination, but also microbial entrapment within an amyloid fibril network (36). Our findings suggest fibrillization is also involved in A $\beta$ -mediated agglutination and leads to the entrapment of microbial cells by A $\beta$  fibrils. Based on our findings, we propose a three-stage model for the

protective activity of A $\beta$  in vivo. Our model parallels the agglutination and entrapment actions of amyloidogenic HD6 (36). First, the VHHQKL heparin-binding domain of A $\beta$  mediates targeting and binding of soluble oligomeric species to cell wall carbohydrates (fig. S10A). Bound oligomers then provide a nidus and anchor for A $\beta$  fibril propagation. Second, growing protofibrils interfere with microbial adhesion to host cells (fig. S10B). Third, A $\beta$  fibrils link, agglutinate, and then entrap the unattached microbial cells in a protease-resistant network  $\beta$ -amyloid (fig. S10C). Consistent with our model for the antimicrobial activities of A $\beta$ , classical human AMPs have also been shown to generate amyloid fibrils on microbial surfaces that agglutinate pathogens and inhibit infection (35).

Consistent with our AMP model for A $\beta$ , APP-KO mice show a trend for reduced pathogen resistance (Fig. 1E). However, the increase in infection-driven mortality among APP-KO mice was less dramatic than the increase in survival observed in the 5XFAD mouse model (Fig. 1A). For AMP-deficient models immune impairment is often moderate because redundant activities among related members of antimicrobial peptide families can partially offset the loss of protection associated with low expression of individual AMP species (50). The well-studied human antimicrobial peptide LL-37 that serves as our model for A $\beta$ 's AMP activity (3) is a member of the cathelicidin protein family. In humans, serious immunodeficiency associated with low LL-37 expression typically leads to fatal infections in childhood if untreated (37). However, mice lacking the murine LL-37 precursor protein (mCRAMP) show only a modest increase in mortality ( $\approx 10\%$ ) with bacterial meningitis (51). Conversely, survival with infection among transgenic mice over-expressing human LL-37 is increased several-fold (52). APP-KO mice generate at least two A $\beta$  homologues from amyloid precursor-like protein one (APLP1) and two (APLP2), which may help to mitigate loss of A $\beta$ -mediated protection (53). Consistent with this model, APP, APLP1, and APLP2 and their non-amyloidogenic processing products show extensive functional redundancy (54), likely because of the gene duplication origin for this protein family. APP-KO mice also have an important additional limitation as models for the loss of A $\beta$ -mediated protection. APP itself may be involved in CNS immunity (55). It remains unclear how loss of activities normally mediated by full-length APP can be excluded as the source of attenuated infection resistance in APP-KO mice.

Genetically modified mice that lack proteases (BACE1 and BACE2) for generating the A $\beta$  family of peptides provide an alternative A $\beta$ -null model. Consistent with our data, knockout BACE-KO mice that lack BACE have been reported to have dramatic immunodeficiency. While neonatal mortality is below two percent under sterile conditions, in less stringently antiseptic environments, up to half of pups born to BACE-KO mice die from infections within the first two-weeks of life (56). Benchmark tests for adaptive immunity have failed to identify defects in the response of BACE-KO mice to immune challenges. Findings for BACE-KO mice appear consistent with an innate immune deficiency and a possible normal protective role for A $\beta$ . However, as with APP-KO mice, it is unclear how to demonstrate that the immunodeficiency in BACE-KO mice is specific for a loss of members of the A $\beta$  family of peptides. Additional data is required to conclusively link the etiology of BACE-KO mouse immunodeficiency to low A $\beta$ .

Our findings for A $\beta$  and  $\beta$ -amyloid may have corollaries for amyloidopathies beyond AD. Protein fibrillization may be important not only for A $\beta$ 's AMP activities, but also for the normal actions of other amyloidosis-causing proteins. An association between amyloidosis and chronic bacterial infections has been recognized for almost a century (57), but the potential protective activities of host-generated amyloid have only recently emerged (4, 35, 58). At least six amyloidosis-associated peptides show antimicrobial activities, including amylin (59), atrial natriuretic factor (9), prion protein (60), cystatin C (61), lysozyme (5), and superoxide dismutase (62). Conversely, host AMPs have been identified that generate protective amyloids localized to infection sites (63). AA type amyloidosis involves both systemic deposition of the acute-phase opsonin AMP serum amyloid A and has an infection-driven etiology (64). It remains to be determined whether serum amyloid A or other amyloidosis-causing AMPs also engage in non-pathogenic fibrillization pathways that help to protect against infection. However, should this prove to be the case, A $\beta$  may be the first member of a new class of AMPs in which amyloid-generating activities protect against local infections, but can also lead to widespread pathological amyloidosis.

If confirmed, our model carries important implications for understanding the pathogenesis of amyloidosis in AD. Excessive  $\beta$ -amyloid deposition may arise not from an intrinsically abnormal propensity of A $\beta$  to aggregate, but instead, may be mediated by dysregulation of the brain's innate immune system, e.g. the consequence of an immune response mounted to microbial or sterile inflammatory stimuli. Importantly, our new model is congruent with the amyloid hypothesis and the importance of A $\beta$  and  $\beta$ -amyloid in the neurodegenerative cascade of AD. However, our model would shift the modality of A $\beta$ 's pathophysiology from abnormal stochastic behavior toward dysregulated antimicrobial activities.

Our study employed genetically modified cell and animal models to generate data consistent with a normal physiological role for A $\beta$  as an AMP. However, it remains unclear from these data how important a role A $\beta$  plays in normal infection resistance. To address this question, additional data will be needed from wild-type animals modeling common physiological routes of infection. Further investigation will also be needed to clarify the extent to which the normal antimicrobial activities of A $\beta$  identified in our study impact AD pathology.

It is important to emphasize that while infection of 5XFAD mice with *S. Typhimurium* seeded and accelerated  $\beta$ -amyloid deposition, the presence of a CNS infection is not implicit in our proposed AD amyloidosis model. Our work has identified what we believe is the normal role of A $\beta$ . What drives widespread  $\beta$ -amyloid deposition in AD remains unclear. Among sterile inflammatory diseases dysregulated innate immune responses rather than infections are emerging as drivers of pathology. Notably, two of the three confirmed AMP amyloidopathies are not linked to obvious infections (4, 9, 65). However, a large body of data accrued over nearly a century suggests that genuine infection may also play a role in AD etiology (66). Moreover, while a causal link to amyloidosis remains to be conclusively demonstrated recent epidemiological findings have given increased prominence to the "infection hypothesis", including studies linking brain fungal infection to AD (17, 18) and data showing risk for the disease increases with infectious burden (67). Our findings do not constitute direct evidence of a role for infection in AD etiology. However, they do suggest a possible mechanism for pathogen-driven  $\beta$ -amyloid amyloidosis. Our data also suggest the

possibility that a range of microbial organisms may be able to induce  $\beta$ -amyloid deposition, a possible reason for why a single pathogen species has not yet been identified that is overwhelmingly associated with AD. Future studies systematically characterizing microbial pathogens (viral, bacterial, fungal) in the brains of AD patients, e.g. by RNASeq, will be necessary to further interrogate whether specific clinical pathogens seed  $\beta$ -amyloid as part of the brain's innate immune system. In any case, whether infectious or sterile inflammatory stimuli drive AD pathology the pathways that regulate innate immunity in the brain may offer significant new targets for therapeutic intervention.

## Materials and Methods

### Study Design

Protective activities associated with A $\beta$ -expression were investigated in murine, nematode, and cell culture models of infection. Transgenic mice, nematode, and cell culture models were used that constitutively express human A $\beta$  at high levels. Experiments also included a null-A $\beta$  mouse model. Modulation of infection resistance with peptide expression is considered a hallmark for identity as an AMP. Initial experiments tested for A $\beta$ -mediated increase (high expression models) or decrease (null-A $\beta$  mice) in survival after infection. Endpoints were death for cultured cells and nematodes and moribundity for mice in accordance with Institutional Animal Care and Use Committee (IACUC) guidelines. Experiments were conducted blind as to cell, nematode, and mouse genotypes. The mechanism of protection afforded by high A $\beta$  expression was then characterized in our cell culture monolayer infection model. We have previously shown parallels between A $\beta$  activities and LL-37, a highly characterized human AMP. LL-37 was used as a model to elucidate the mechanisms for A $\beta$ 's targeting, adhesion inhibition and agglutination activities against microbial cells. Finally, nematode and mice models were tested to confirm in animals the potential protective microbial entrapment role of A $\beta$  fibrillization revealed by cell culture experiments. Figure legends include details of replicate experiments used to generate data sets.

### Monomeric and oligomeric synthetic peptide preparation

Synthetic A $\beta$ 1–40 (A $\beta$ 40), A $\beta$ 1–42 (A $\beta$ 42), scrambled A $\beta$ 42 (scA $\beta$ 42), and LL-37 peptides were prepared and purified by Dr. James I. Elliott at Yale University (New Haven, CT) using solid-phase peptide synthesis. Bulk powdered A $\beta$  peptides were initially dissolved and incubated (18 hrs) at room temperature (RT) in 30% trifluoroethanol (1 mg/ml) prior to lyophilization and storage ( $-20^{\circ}\text{C}$ ) under nitrogen. Prior to experimentation dried peptide films were solubilized in 10 mM NaOH. For preparation of monomeric A $\beta$  stocks, peptide solutions were diluted into phosphate-buffered saline (PBS), fractionated by SEC, and peak monomer fractions (3–6 kDa) pooled. Monomer stocks were stored on ice at 100  $\mu\text{M}$  and used within 2 hrs of preparation. Synthetic A $\beta$ 42 oligomer preparations (ADDLs and protofibrils) were generated from NaOH peptide stocks using established protocols (68). Peptide concentrations in stock solutions were determined by bicinchoninic acid protein assay and confirmed in experimental serial dilutions by densitometry analysis of anti-A $\beta$  immunoblots.

### **Candida inoculants and lawns**

Freezer stocks of *Candida albicans* strain 90028 were obtained from the American Type Culture Collection (ATCC) (Manassas, VA). *C. albicans* stocks were maintained on yeast extract peptone dextrose (YPD) agar at 4 °C with subculture to fresh plates every two weeks.

*C. elegans* pathogenicity plates were prepared by streaking (10 µl) sterile 35m tissue culture plates (BD Falcon) with yeast grown overnight (30 °C) in YPD broth. Plates were incubated at 25 °C for 2 hrs to generate *C. albicans* lawn.

Synchronized hyphal yeast for cell culture experiments were prepared by single colony transfer of *C. albicans* stock to 5 mls of Minimal Sugar Medium (*Formedium*) and 48 hr static incubation at RT (69). After pelleting (1,750 RCF for 2 mins) and PBS washing, starved yeast were resuspended in RPMI-1640 medium (Hyclone, Logan, UT) and concentration adjusted to  $2.5 \times 10^6$  cells/ml. Stock yeast in RPMI were diluted 10-fold into unconditioned culture media immediately prior to inoculation of host cell slide or culture plate wells. Yeast concentration in inoculates was determined using a BioRad TC20 automated cell counter and confirmed by counting CFU after serial dilution and streaking on agar.

### **S. Typhimurium inoculants**

*Salmonella enterica* serotype Typhimurium SL1344 stocks were kindly provided by Dr Bobby Cherayil (Mucosal Immunology Department, Massachusetts General Hospital, Boston MA). Colonies were maintained on agar and subcultured to fresh plates every three weeks. Inoculant stocks were prepared by single *S. Typhimurium* colony to transfer to Luria-Bertani (LB) agar with 100 µg/ml streptomycin and incubation overnight in a shaker incubator (225 rpm at 37 °C). After PBS washing, pelleted (10,000g × 2 min) bacteria were resuspended in inoculation media, and diluted to required concentration. Bacterial concentrations in stocks were determined by comparing inoculum turbidity to McFarland turbidity standards and confirmed by streaking on agar and counting CFU.

For mouse experiments, *S. Typhimurium* inoculants were pathologized prior to infection by incubation (90 min at 37 °C) in a CO<sub>2</sub> atmosphere. Pathogenicity plates for *C. elegans* were prepared by streaking inoculate (10 µl) onto *Pseudomonas aeruginosa*- and *Salmonella enterica*-killing assay (SK) plates and overnight incubation at 37 °C. For HCMs, inoculant was added directly to the culture media of host cells.

### **Immunodepletion**

Protein G Plus Agarose slurry (Pierce, IL) was pelleted, washed and incubated for 2 hrs at RT with 4G8 (epitope: Aβ17–24) monoclonal antibody (Covance, Princeton, NJ) or control mouse IgG in PBS. After washing, beads were incubated with media samples for 2 hrs at RT under conditions equivalent to 10 µg of antibody per ml of media. Beads were pelleted and soluble fractions were removed, filtered (0.2 µm), and assayed to confirm Aβ depletion.

## A $\beta$ binding ELISA

The wells of 96-well plates were coated with live yeast by overnight incubation (37° C) with synchronized *C. albicans* (50–250 CFU's/well) in RPMI media (200  $\mu$ l/well). Wells were washed to remove unattached yeast and adhering *C. albicans* cells then killed and covalently fixed in place by incubation (15 min at RT) with 4 % paraformaldehyde. Wells were blocked (2 hrs at RT) with 2 % BSA in PBS prior to incubation with experimental samples. Bound A $\beta$  in wells was detected immunochemically by incubation (overnight at 4° C) with  $\alpha$ -A $\beta$ 42-HRP (Covance) diluted 1:1,000 in blocking buffer and development with 100  $\mu$ l of chemiluminescence reagent (Pierce, Rockford IL). Wells were washed (x5) with PBS between incubations.

## Mouse infection model

Female 5XFAD(12) APP/PS1 doubly transgenic mice that co-overexpress and co-inherit FAD mutant forms of human APP (the Swedish mutation: K670N, M671L; the Florida mutation: I716V; the London mutation: V717I) and PS1 (M146L; L286V) transgenes under transcriptional control of the neuron-specific mouse Thy-1 promoter (Tg6799 line). 5XFAD lines (B6/SJL genetic background) were purchased from Jackson Laboratory and maintained by crossing heterozygous transgenic mice with B6/SJL F1 breeders. All 5XFAD transgenic mice were heterozygotes with respect to the transgene. Animal experiments were conducted in accordance with institutional and NIH guidelines.

One-month old mice received a single injection of 65,000 CFU (0.18–0.20 ml) of *S. Typhimurium* suspension at AP, -1.6; ML, +1.5; DV, -1.6/-1.1/-0.7 using a 5  $\mu$ l Hamilton syringe with a 30-gauge needle attached to a digital stereotaxic apparatus and an infusion pump at a rate of 0.15  $\mu$ l/min. After infusion was completed, the needle remained in place for 10 min before slow withdrawal. Mice were given food and water on the cage floor starting 24 hrs after the injection. Control sham infections used *S. Typhimurium* heat-killed prior to injection.

Clinical scores were recorded every 8 hrs according to a modified grading criteria for mouse encephalomyelitis (70, 71). Clinical criteria are summarized in Fig. S1a. Clinical progression was followed to moribundity and then mice were sacrificed. Scores were recorded for each mouse and expressed as mean  $\pm$  SEM.

## Mouse tissue preparation and sectioning

For immunofluorescence, mice were deeply anesthetized with a mixture of ketamine and xylazine, and perfused transcardially with 4% paraformaldehyde in cold PBS. Brains were postfixed overnight and then transferred into a 30% sucrose solution until sedimented. Coronal sections (40  $\mu$ m) were cut from an ice-cooled block using a sliding microtome (Leica, Wetzlar, Germany). Sections were stored at -20°C in cryoprotective buffer containing 28% ethylene glycol, 23% glycol and 0.05 M phosphate until processing for analysis.

### Immunofluorescence labeling of mouse sections

Immunofluorescence labeling was performed as previously described (12). Primary antibodies include, rabbit anti-GFAP (1:500, Dako, Fort Collins, CO) for astrocytes, rabbit anti-ionized calcium-binding adaptor molecule 1 (Iba1, 1:500, Wako, Osaka, Japan) for microglia, and anti-*Salmonella* polyclonal rabbit for *S. Typhimurium*. Bound primary antibodies were detected with anti-rabbit Alexafluor 594 (Invitrogen, 8889S). Cell nuclei in sections were stained with TO-PRO®-3 iodide (1:500, Life technologies, Eugene, OR).

### Immuno- and Thioflavin S-costained mouse sections

Immunofluorescence labeling was performed as described previously (72). Briefly, sections were incubated with primary anti-*Salmonella* polyclonal rabbit IgG (1:1000) (PA1-7244, ThermoFisher Scientific) followed by secondary anti-rabbit Alexafluor 594 (1:500) (Invitrogen, 8889S) antibodies. For A $\beta$  staining sections were incubated with mouse monoclonal antibodies 3D6 (Eli Lilly) (mouse brain sections) or 4G8 (nematode sections). Bound anti-A $\beta$  antibodies were detected by incubation with anti-mouse Alexafluor 488 (1:500) (Life Technologies, A11001) antibodies (Invitrogen). After immunostaining, free-floating sections were incubated (8 min) with 0.002% Thioflavin S in TBS, rinsed twice for 1 min in 50% ethanol, washed for 5 min in TBS, and mounted with Prolong Gold antifade reagent (Life Technologies). Stained sections were analyzed by fluorescence confocal microscopy (Leica TCS SL, Leica Microsystems, Germany).

### *C. elegans* model

Two previously described transgenic *C. elegans* strains were used in experiments. GMC101, *dvIs100* [pCL354(*unc-54:DA-A $\beta$ 1-42*) + pCL26 (*mtl-2: GFP*)] nematodes express human A $\beta$ 42 in body wall muscle and green fluorescent protein (GFP) in intestinal cells (14). Control *C. elegans* CL2122 *dvIs15*(*mtl-2: GFP*) nematodes express GFP but not the A $\beta$ 42 peptide (14). Worm were synchronization prior to experimental treatments according to established protocols (73). Briefly, unhatched eggs were release by treating gravid worms with bleach. After an overnight incubation, arrested L1 larvae were added to *E. coli* OP50 lawns and incubated at 20 °C to generate synchronized L4 larval (48 hrs) or adult (60 hrs) nematodes.

For infection experiments, 100–150 synchronized L4 stage worms were incubated (2 hrs at 25 °C) on *C. albicans* lawns, washed with M9 buffer to remove surface *C. albicans*, and transferred to 6-well culture plates containing 1.5 ml/well of incubation media (79 % M9 buffer, 20% BHI, 10  $\mu$ g/ml cholesterol in ethanol, and 90  $\mu$ g/ml kanamycin). Nematodes were incubated at 25 °C and monitored daily for the distinctive distention and penetrative filamentation that characterizes *Candida*-induced mortality.

### Nematode freeze-fracture and immunostaining

Worms (L4) were transferred dropwise to poly-lysine coated slides and covered with a coverslip. Gentle pressure was applied to the coverslip before the slide assembly was placed on a metal block and flash-frozen using liquid nitrogen. The coverslip was flicked off and fractured samples fixed by 5 min incubations with absolute alcohol followed by acetone. Dried samples were ringed with petroleum jelly and covered with a second coverslip. Slide



staining was performed in a wet chamber. For immunostaining, slides were blocked for 15 min with blocking buffer (10 % tween and 0.2 g/ml powdered milk in PBS) then incubated (1 hr at RT) with rabbit polyclonal anti-*Candida* antibody (Abcam, ab20028) and/or anti-A $\beta$  mAb 4G8. After washing, slides were incubated with anti-rabbit and/or anti-mouse antibodies conjugated to AlexaFluor 568 and AlexaFluor 488 fluorescent dyes (Life Technologies), respectively. For Thioflavin S staining, slides were incubated 1 hr at RT with dye solution and PBS washed. Specimens were incubated with prolong Gold antifade reagent (Life Technologies) before viewing by CFM.

### Host cell monolayer model

Host cell monolayers were prepared from non-transformed and transformed human neuroglioma (H4) or Chinese hamster ovary (CHO) cell lines. Stable transformed H4 cell lines that secrete A $\beta$ 40 (H4-A $\beta$ 40) or A $\beta$ 42 (H4-A $\beta$ 42) without over expression of the APP have been described previously (19). Stable transformed CHO-CAB cells co-expressing human ATCC Swedish mutation and  $\beta$ -site APP cleaving enzyme 1 (BACE1) were generated by transfecting a pcDNA3.1-BACE1-myc construct into CHO-APP751 cells that over-express mutant APP751 (K670N/M671L: Swedish mutation) (20).

Non-transformed H4-N and CHO-N cell lines were maintained in complete media containing DMEM, 10% Fetal Bovine Serum (FBS), 2 mM L-glutamine, 100 U penicillin, and 100  $\mu$ g/ml streptomycin. Complete media for transformed H4-A $\beta$ 40 and H4-A $\beta$ 42 cells included hygromycin (150  $\mu$ g/ml) and media for CHO-CAB Zeocin (200  $\mu$ g/ml) and G418 (200  $\mu$ g/ml).

To prepare experimental HCMs, trypsinized host cells suspended in antibiotic-free DMEM with 5 % FBS and 2 mM L-glutamine were transferred (300,000 and 500,000 cells/ml for H4 and CHO lines, respectively) to the wells of Lab-Tek 8-chamber glass slides (Thermo Scientific, Waltham, MA) (200  $\mu$ l/well) or 96-well culture plates (100  $\mu$ l/well) and incubated for 24 hrs. Cell confluence in chamber slides and plate wells were confirmed by microscopic examination. Automated cell counter analysis of well trypsin extracts confirmed that in control uninfected HCMs non-transformed and transformed cell numbers did not diverge by more than 6 % prior to infection, or after the final experimental incubation (Fig. S4D).

Non-transformed and transformed culture media were conditioned for 36 hrs before inoculation with *Candida*. HCM in culture plates were infected by addition of *Candida* inoculant aliquots (10  $\mu$ l) containing 2,000 or 250,000 CFU, respectively. For host cell survival experiments, *Candida* were incubated with H4 and CHO cells for 28 and 36 hours, respectively. HCMs were then washed and assayed for host cell survival.

### Host cell BrdU labeling

Subconfluent non-transformed and transformed H4 and CHO cells were incubated overnight (10 cm culture dishes) in complete culture media containing 10 mM BrdU. Confluent BrdU-labeled cell cultures were PBS washed (x3) to remove free BrdU then trypsinized and used for preparation of HCMs in 96-well culture plates. After experimental treatments, plate wells were washed with PBS (x3) then fixed and permeabilized, and assayed according to manufacture's instructions (Cell Proliferation BrdU ELISA, Roche).

### Imaging *C. albicans* host cell adherence

HCMs in 8-well chamber slides were infected with synchronized hyphal yeast (10,000 CFU/well) by addition of a 10  $\mu$ l aliquot of freshly prepared *C. albicans* inoculate to culture media (200  $\mu$ l/well) pre-conditioned for 36 hrs with host cells. Infected slides were incubated for 2 hrs, media removed by aspiration, wells washed with PBS (x3) and then fixed by 10 min incubation with 4 % paraformaldehyde. Fixative was removed and wells washed (x3) before incubation (30 min) with Calcofluor white M2R fungal surface stain (74) (Life Technologies). Wells were water washed and coverslipped before imaging by fluorescence microscopy (Ex360 nm/Em460 nm).

### Immunochemical detection of *C. albicans* adhering to host cell monolayers

Experiments were performed using HCMs prepared in white opaque 96-well culture plates. HCMs were infected with synchronized hyphal yeast (1,000 CFU/well) by addition of 10  $\mu$ l of freshly prepared *C. albicans* inoculate to wells containing pre-conditioned (36 hrs) culture media (100  $\mu$ l/well). Wells were incubated 18 hrs with yeast before aspiration of media, gentle washing with PBS (x3), and fixation by 10 min incubation with 4 % paraformaldehyde. Fixative was removed and wells washed (x3) before incubation (1 hr) with blocking buffer (2 % albumin in TBST). Wells were then incubated (2 hrs) with fresh blocking buffer containing a 1:5000 dilution of  $\alpha$ -*Candida*-HRP antibody (Abcam, Boston MA). Wells were washed with TBST (x5) and fluorescent captured (Ex320 nm/Em420 nm) after development with QuantaBlu (Pierce, Rockford IL), a fluorescent HRP substrate.

### *C. albicans* adhesion assay for abiotic surfaces

Experiments used a modified method of Tsai *et al*, 2011(22) to assay *C. albicans* adhesion to polystyrene in conditioned culture media. Synchronized hyphal yeast (1000 CFU/well) were incubated (37° C) in the wells of clear flat-bottom polystyrene 96-well microtiter plates containing host cell conditioned (36 hrs) culture media (200  $\mu$ l/well). Incubation media was removed by aspiration and wells washed (x3) before incubation (30 min at RT) with PBS (200  $\mu$ l/well) containing 10  $\mu$ l of Calcofluor white fungal stain solution 6726 (ENG Scientific, Clifton, NJ). After washing, attached hyphae were detected by measuring well fluorescence (Ex360 nm/Em460 nm).

### *C. albicans* aggregation assay

Host cell conditioned (48 hrs) culture media (200  $\mu$ l/well) was incubated (overnight at 37° C) with synchronized yeast (200 cells/well) in the wells of clear 96-well microtiter plates. Incubation media was removed and yeast pellets washed twice with PBS. During aspiration care was taken to minimize disturbance of settled yeast at the well bottom. Settled yeast pellets were resuspended in PBS and transferred to fresh wells. Low magnification (x4) bright field well images were captured at maximum condenser aperture. Images were then analyzed for yeast aggregates using ImageJ software (version 1.47) with the following procedure. Captured image files were first converted from 8-bit RGB to 8-bit greyscale then further transformed to 1-bit black and white images using a conversion threshold of 86%. Well area covered by yeast aggregates was determined from pixel counts of transformed black and white images using the Analyze Particle tool with lower size threshold set to 50

pixels. Isolated black areas of less than 50 pixels (4–6 yeast cells) were not included in aggregate totals.

### Staining and antibody labeling of *C. albicans* aggregates

Aggregated yeast were pelleted (2 min  $\times$  500 *g*), washed with PBS (x2), transferred to glass slides in minimal volume, and excess buffer blotted off. Slides were air-dried to fix yeast and then carefully rinsed with water. For dye staining, slides were incubated in the dark at RT with 50  $\mu$ l of Thioflavin S (5 min) or staining solution then water rinsed. For immunolabeling experiments specimens pre-stained with Thioflavin S were incubated (2 hrs at 4° C) with blocking buffer containing 1:1,000 dilution of mAb 4G8. Slides were TBST rinsed and then incubated (1 hr at RT) with donkey anti-mouse-IgG antibody covalently labeled with the red-fluorescent dye Alexa Fluor 594 ( $\alpha$ -mouse-AF568) (Life Technologies). Thioflavin and anti-A $\beta$  double labeled specimens were mounted with Prolong Gold antifade reagent (Life Technologies) before viewing with a fluorescence confocal microscope (Leica TCS SL, Leica Microsystems, Germany).

### TEM of microbial agglutinates

*Candida* aggregates cells suspended in PBS (5  $\mu$ l) were absorbed to Formvar carbon coated copper grids (FCF100-Cu, Electron Microscopy Sciences, Hatfield, PA). Grids were blocked with 1 % BSA in PBS (kept covered for 10 min at RT) then incubated (30 min at RT) with mAb 4G8 diluted 1:1,000 in blocking buffer. Grids were washed with PBS (x3) and incubated with goat anti-mouse-IgG antibody covalently linked to nanogold particles. After three 5 min PBS washes and four 10 min water washes, specimens were fixed with 1 % glutaraldehyde (10 min at RT). Specimens were washed with water, stained with uranyl acetate, and then viewed using a JEM-1011 Transmission Electron Microscope (JEOL Institute, Peabody, MA).

### Statistical analysis

Statistical analyses were performed with Prism software (version 6.0c). Arithmetic means were compared using two tailed t-tests. Survival curves were compared using Log-rank (Mantel-Cox) test and confirmed by Gehan-Breslow-Wilcoxon test. *P* values < 0.05 were considered statistically significant.

### Supplementary Material

Refer to Web version on PubMed Central for supplementary material.

### Acknowledgments

The authors would like to thank Todd Golde for the A $\beta$ -expressing transfected cell line and Ashley Bush for transgenic nematodes. No patents have been filed in associated with this work. The authors have also not been engaged for consulting purposes nor own companies related to this work

**Funding:** This work was supported by grants from NIH (5R01AI081990-02), the Cure Alzheimer's Fund, and The Helmsley Charitable Trust.

## References

1. Tanzi RE, Bertram L. Twenty years of the Alzheimer's disease amyloid hypothesis: a genetic perspective. *Cell*. 2005; 120:545–555. [PubMed: 15734686]
2. Luna S, Cameron DJ, Ethell DW. Amyloid- $\beta$  and APP deficiencies cause severe cerebrovascular defects: important work for an old villain. *PLoS ONE*. 2013; 8:e75052. [PubMed: 24040383]
3. Soscia SJ, Kirby JE, Washicosky KJ, Tucker SM, Ingelsson M, Hyman B, Burton MA, Goldstein LE, Duong S, Tanzi RE, Moir RD. The Alzheimer's disease-associated amyloid- $\beta$  protein is an antimicrobial peptide. *PLoS ONE*. 2010; 5:e9505. [PubMed: 20209079]
4. Kagan BL, Jang H, Capone R, Teran Arce F, Ramachandran S, Lal R, Nussinov R. Antimicrobial properties of amyloid peptides. *Mol Pharm*. 2012; 9:708–717. [PubMed: 22081976]
5. Wiesner J, Vilcinskas A. Antimicrobial peptides: the ancient arm of the human immune system. *Virulence*. 2010; 1:440–464. [PubMed: 21178486]
6. Yamaguchi Y, Nagase T, Tomita T, Nakamura K, Fukuhara S, Amano T, Yamamoto H, Ide Y, Suzuki M, Teramoto S, Asano T, Kangawa K, Nakagata N, Ouchi Y, Kurihara H.  $\alpha$ -defensin overexpression induces progressive muscle degeneration in mice. *Am. J. Physiol, Cell Physiol*. 2007; 292:C2141–C2149. [PubMed: 17215327]
7. Reinholz M, Ruzicka T, Schaubert J. Cathelicidin LL-37: an antimicrobial peptide with a role in inflammatory skin disease. *Ann Dermatol*. 2012; 24:126–135. [PubMed: 22577261]
8. Cao Y, Chtarbanova S, Petersen AJ, Ganetzky B. Dnr1 mutations cause neurodegeneration in *Drosophila* by activating the innate immune response in the brain. *PNAS*. 2013; 110:E1752–1760.  $\beta$ . [PubMed: 23613578]
9. Krause A, Liepke C, Meyer M, Adermann K, Forssmann WG, Maronde E. Human natriuretic peptides exhibit antimicrobial activity. *Eur. J. Med. Res*. 2001; 6:215–218. [PubMed: 11410403]
10. White MR, Kandel R, Tripathi S, Condon D, Qi L, Taubenberger J, Hartshorn KL. Alzheimer's associated  $\beta$ -amyloid protein inhibits influenza A virus and modulates viral interactions with phagocytes. *PLoS ONE*. 2014; 9:e101364. [PubMed: 24988208]
11. Bourgade K, Garneau H, Giroux G, Le Page AY, Bocti C, Dupuis G, Frost EH, Fulop T Jr.  $\beta$ -Amyloid peptides display Alzheimer's disease-associated herpes simplex virus-1. *Bioger ontology*. 2015; 16:85–98.
12. Oakley H, Cole SL, Logan S, Maus E, Shao P, Craft J, Guillozet-Bongaarts A, Ohno M, Disterhoft J, Van Eldik L, Berry R, Vassar R. Intraneuronal  $\beta$ -amyloid aggregates neurodegeneration and neuron loss in transgenic mice. *J Neurosci*. 2006; 26:10129–10140. [PubMed: 17021169]
13. Zheng H, Jiang M, Trumbauer ME, Hopkins R, Sirinathsinghji DJ, Stevens KA, Conner MW, Slunt HH, Sisodia SS, Chen HY, Van der Ploeg LH. Mice deficient for the amyloid precursor protein gene. *Ann N Y Acad Sci*. 1996; 777:421–426. [PubMed: 8624124]
14. McColl G, Roberts BR, Pukala TL, Kenche VB, Roberts CM, Link CD, Ryan TM, Masters CL, Barnham KJ, Bush AI, Cherny RA. Utility of an improved model of amyloid- $\beta$  ( $\beta$ 1–42) toxicity in *Caenorhabditis elegans* for drug screening for Alzheimer's disease. *Mol Neurodegener*. 2012; 7:57. [PubMed: 23171715]
15. Ardizzi JP, Epstein HF. Immunohistochemical localization of myosin heavy chain isoforms and paramyosin in developmentally and structurally diverse muscle cell types of the nematode *Caenorhabditis elegans*. *J Cell Biol*. 1987; 105:2763–2770. [PubMed: 3320053]
16. Nussbaum-Krammer CI, Park KW, Li L, Melki R, Morimoto RI. Spreading of a prion domain from cell-to-cell by vesicular transport in *Caenorhabditis elegans*. *PLoS Genet*. 2013; 9:e1003351. [PubMed: 23555277]
17. Pisa D, Alonso R, Rabano A, Rodal I, Carrasco L. Different Brain Regions are Infected with Fungi in Alzheimer's Disease. *Sci Rep*. 2015; 5:15015. [PubMed: 26468932]
18. Alonso R, Pisa D, Marina AI, Morato E, Rábano A, Carrasco L. Fungal infection in patients with Alzheimer's disease. *J Alzheimers Dis*. 2014; 41:301–311. [PubMed: 24614898]
19. Lewis PA, Piper S, Baker M, Onstead L, Murphy MP, Hardy J, Wang R, McGowan E, Golde TE. Expression of BRI-amyloid- $\beta$  peptide fusion proteins: a novel method for specific high-level expression of amyloid- $\beta$  peptides. *Biochim Biophys Acta*. 2001; 1537:58–62. [PubMed: 11476963]

20. Hahn S, Brüning T, Ness J, Czirr E, Baches S, Gijzen H, Korth C, Pietrzik CU, Bulic B, Weggen S. Presenilin-1 but not amyloid precursor protein mutations present in mouse models of Alzheimer's disease attenuate the response of cultured cells to  $\gamma$ -secretase modulators regardless of their potency and structure. *J Neurochem.* 2011; 116:385–395. [PubMed: 21091478]
21. Hock C, Golombowski S, Müller-Spahn F, Naser W, Beyreuther K, Mönning U, Schenk D, Vigo-Pelfrey C, Bush AM, Moir R, Tanzi RE, Growdon JH, Nitsch RM. Cerebrospinal fluid levels of amyloid precursor protein and amyloid  $\beta$ -peptide in Alzheimer's disease and major depression - inverse correlation with dementia severity. *Eur Neurol.* 1998; 39:111–118. [PubMed: 9520072]
22. Tsai P-W, Yang C-Y, Chang H-T, Lan C-Y. Human antimicrobial peptide LL-37 inhibits adhesion of *Candida albicans* by interacting with yeast cell-wall carbohydrates. *PLoS ONE.* 2011; 6:e17755. [PubMed: 21448240]
23. Weidner AM, Housley M, Murphy MP, LeVine H. Purified high molecular weight synthetic A $\beta$  (1-42) and biological A $\beta$  oligomers are equipotent in rapidly inducing MTT formazan exocytosis. *Neurosci Lett.* 2011; 497:1–5. [PubMed: 21504780]
24. Lambert MP, Barlow AK, Chromy BA, Edwards C, Freed R, Liosatos M, Morgan TE, Rozovsky I, Trommer B, Viola KL, Wals P, Zhang C, Finch CE, Krafft GA, Klein WL. Diffusible nonfibrillar ligands derived from A $\beta$ 1-42 are potent central nervous system neurotoxins. *Proc Natl Acad Sci USA.* 1998; 95:6448–6453. [PubMed: 9600986]
25. Yang T, Hong S, Malley TO, Sperling RA, Walsh DM, Selkoe DJ. New ELISAs with high specificity for soluble oligomers of amyloid- $\beta$  protein detect natural A $\beta$  oligomers in human brain but not CSF. *Alzheimers Dement.* 2013
26. Sood R, Domanov Y, Pietiäinen M, Kontinen VP, Kinnunen PKJ. Binding of LL-37 to model biomembranes: insight into target vs host cell recognition. *Biochim Biophys Acta.* 2008; 1778:983–996. [PubMed: 18166145]
27. Feder R, Dagan A, Mor A. Structure-activity relationship study of antimicrobial dermaseptin S4 showing the consequences of peptide oligomerization on selective cytotoxicity. *J Biol Chem.* 2000; 275:4230–4238. [PubMed: 10660589]
28. Leonova L, Kokryakov VN, Aleshina G, Hong T, Nguyen T, Zhao C, Waring AJ, Lehrer RI. Circular minidefensins and posttranslational generation of molecular diversity. *J Leukoc Biol.* 2001; 70:461–464. [PubMed: 11527997]
29. Lehrer RI. Paradise lost and paradigm found. *Nat Immunol.* 2004; 5:775–776. [PubMed: 15282557]
30. Sal-Man N, Oren Z, Shai Y. Preassembly of membrane-active peptides is an important factor in their selectivity toward target cells. *Biochemistry.* 2002; 41:11921–11930. [PubMed: 12269837]
31. Watson DJ, Lander AD, Selkoe DJ. Heparin-binding properties of the amyloidogenic peptides A $\beta$  and amylin. Dependence on aggregation state and inhibition by Congo red. *J Biol Chem.* 1997; 272:31617–31624. [PubMed: 9395501]
32. Tsai P-W, Yang C-Y, Chang H-T, Lan C-Y. Characterizing the role of cell-wall  $\beta$ -1,3-exoglucanase Xog1p in *Candida albicans* adhesion by the human antimicrobial peptide LL-37. *PLoS ONE.* 2011; 6:e21394. [PubMed: 21713010]
33. Calvete JJ, Campanero-Rhodes MA, Raida M, Sanz L. Characterisation of the conformational and quaternary structure-dependent heparin-binding region of bovine seminal plasma protein PDC-109. *FEBS Lett.* 1999; 444:260–264. [PubMed: 10050771]
34. van Horsen J, Wesseling P, van den Heuvel LPWJ, de Waal RMW, Verbeek MM. Heparan sulphate proteoglycans in Alzheimer's disease and amyloid-related disorders. *Lancet Neurol.* 2003; 2:482–492. [PubMed: 12878436]
35. Torrent M, Pulido D, Nogués MVr, Boix E. Exploring new biological functions of amyloids: bacteria cell agglutination mediated by host protein aggregation. *PLoS Pathog.* 2012; 8:e1003005. [PubMed: 23133388]
36. Chu H, Pazgier M, Jung G, Nuccio S-P, Castillo PA, de Jong MF, Winter MG, Winter SE, Wehkamp J, Shen B, Salzman NH, Underwood MA, Tsois RM, Young GM, Lu W, Lehrer RI, Bäuml AJ, Bevins CL. Human  $\alpha$ -defensin 6 promotes mucosal innate immunity through self-assembled peptide nanonets. *Science.* 2012; 337:477–481. [PubMed: 22722251]

37. Pütsep K, Carlsson G, Boman HG, Andersson M. Deficiency of antibacterial peptides in patients with morbus Kostmann: an observation study. *Lancet*. 2002; 360:1144–1149. [PubMed: 12387964]
38. Ciornei CD, Tapper H, Bjartell A, Sternby NH, Bodelsson M. Human antimicrobial peptide LL-37 is present in atherosclerotic plaques and induces death of vascular smooth muscle cells: a laboratory study. *BMC Cardiovas Disord*. 2006; 6:49.
39. Kahlenberg JM, Kaplan MJ. Little peptide big effects: the role of LL-37 in inflammation and autoimmune disease. *J Immuno*. 2013; 191:4895–4901.
40. Shinkai Y, Yoshimura M, Morishima-Kawashima M, Ito Y, Shimada H, Yanagisawa K, Ihara Y. Amyloid  $\beta$ -protein deposition in the leptomeninges and cerebral cortex. *Ann Neurol*. 1997; 42:899–908. [PubMed: 9403483]
41. Brandenburg L-O, Varoga D, Nicolaeva N, Leib SL, Wilms H, Podschun R, Wruck CJ, Schröder J-M, Pufe T, Lucius R. Role of glial cells in the functional expression of LL-37/rat cathelin-related antimicrobial peptide in meningitis. *J Neuropathol Exp Neurol*. 2008; 67:1041–1054. [PubMed: 18957897]
42. Wozniak MA, Itzhaki RF, Shipley SJ, Dobson CB. Herpes simplex virus infection causes cellular  $\beta$ -amyloid accumulation and secretase upregulation. *Neurosci Lett*. 2007; 429:95–100. [PubMed: 17980964]
43. Miklossy J. Chronic inflammation and amyloidogenesis in Alzheimer's disease -- role of Spirochetes. *J Alzheimers Dis*. 2008; 13:381–391. [PubMed: 18487847]
44. Boelen E, Stassen FR, van der Ven AJ, Lemmens MA, Steinbusch HP, Bruggeman CA, Schmitz C, Steinbusch HW. Detection of amyloid- $\beta$  aggregates in the brain of BALB/c mice after Chlamydia pneumoniae infection. *Acta Neuropathol*. 2007; 114:255–261. [PubMed: 17581756]
45. Little CS, Hammond CJ, MacIntyre A, Balin BJ, Appelt DM. Chlamydia pneumoniae induces Alzheimer-like amyloid plaques in brains of BALB/c mice. *Neurobiol Aging*. 2004; 25:419–429. [PubMed: 15013562]
46. Papo N, Shai Y. Can we predict biological activity of antimicrobial peptides from their interactions with model phospholipid membranes? *Peptides*. 2003; 24:1693–1703. [PubMed: 15019200]
47. Pomin VH. Heparin-Binding Proteins (Chemokines and Defensins) and their complexes with glycosaminoglycans from the solution NMR perspective. *Curr Protein Pept Sci*. 2014; 15:738–744. [PubMed: 25175334]
48. Wang J, Li Y, Wang X, Chen W, Sun H, Wang J. Lipopolysaccharide induces amyloid formation of antimicrobial peptide HAL-2. *Biochim Biophys Acta*. 2014; 1838:2910–2918. [PubMed: 25109934]
49. Goldmann O, Medina E. The expanding world of extracellular traps: not only neutrophils but much more. *Front Immunol*. 2012; 3:420. [PubMed: 23335924]
50. Wilson SS, Wiens ME, Smith JG. Antiviral mechanisms of human defensins. *J Mol Biol*. 2013; 425:4965–4980. [PubMed: 24095897]
51. Bergman P, Johansson L, Wan H, Jones A, Gallo RL, Gudmundsson GH, Hökfelt T, Jonsson A-B, Agerberth B. Induction of the antimicrobial peptide CRAMP in the blood-brain barrier and meninges after meningococcal infection. *Infect Immun*. 2006; 74:6982–6991. [PubMed: 17030578]
52. Bals R, Weiner DJ, Moscioni AD, Meegalla RL, Wilson JM. Augmentation of innate host defense by expression of a cathelicidin antimicrobial peptide. *Infect Immun*. 1999; 67:6084–6089. [PubMed: 10531270]
53. Eggert S, Paliga K, Soba P, Evin G, Masters CL, Weidemann A, Beyreuther K. The proteolytic processing of the amyloid precursor protein gene family members APLP-1 APLP-2 involves  $\alpha$ -,  $\beta$ -gamma-and epsilon-like cleavages: modulation of APLP-1 processing by n-glycosylation. *J Biol Chem*. 2004; 279:18146–18156. [PubMed: 14970212]
54. Shariati SA, De Strooper B. Redundancy and divergence in the amyloid precursor protein family. *FEBS Lett*. 2013; 587:2036–2045. [PubMed: 23707420]
55. Beyreuther K, Pollwein P, Multhaup G, Monning U, König G, Dyrks T, Schubert W, Masters CL. Regulation expression of the Alzheimer's  $\beta$ /A4 amyloid protein precursor in health disease and Down's syndrome. *Ann N Y Acad Sci*. 1993; 695:91–102. [PubMed: 8239320]

56. Dominguez D, Tournoy J, Hartmann D, Huth T, Cryns K, Deforce S, Serneels L, Camacho IE, Marjaux E, Craessaerts K, Roebroek AJM, Schwake M, Hooge RD, Bach P, Kalinke U, Moechars D, Alzheimer C, Reiss K, Saftig P, de Strooper B. Phenotypic and biochemical analyses of BACE1- and BACE2-deficient mice. *J Biol Chem*. 2005; 280:30797–30806. [PubMed: 15987683]
57. Falk RH, Comenzo RL, Skinner M. The systemic amyloidoses. *N Engl J Med*. 1997; 337:898–909. [PubMed: 9302305]
58. Kagan BL. Antimicrobial amyloids? *Biophys J*. 2011; 100:1597–1598. [PubMed: 21463571]
59. Wang L, Liu Q, Chen J-C, Cui Y-X, Zhou B, Chen Y-X, Zhao Y-f, Li Y-m. Antimicrobial activity of human islet amyloid polypeptides: an insight into amyloid peptides's; connection with antimicrobial peptides. *Biol Chem*. 2012; 393:641–646. [PubMed: 22944668]
60. Pasupuleti M, Roupe M, Rydengård V, Surewicz K, Surewicz WK, Chalupka A, Malmsten M, Sörensen OE, Schmidtchen A. Antimicrobial activity of human prion protein is mediated by its N-terminal region. *PLoS ONE*. 2009; 4:e7358. [PubMed: 19809501]
61. Vernekar V, Velhal S, Bandivdekar A. Evaluation of cystatin C activities against HIV. *Indian J Med Res*. 2015; 141:423–430. [PubMed: 26112843]
62. Pasupuleti M, Davoudi M, Malmsten M, Schmidtchen A. Antimicrobial activity of a C-terminal peptide from human extracellular superoxide dismutase. *BMC Res Notes*. 2009; 2:136. [PubMed: 19604396]
63. Kagan BL, Jang H, Capone R, Teran Arce F, Ramachandran S, Lal R, Nussinov R. Antimicrobial properties of amyloid peptides. *MolPharm*. 2012; 9:708–717.
64. Shah C, Hari-Dass R, Raynes JG. Serum amyloid A is an innate immune opsonin for Gram-negative bacteria. *Blood*. 2006; 108:1751–1757. [PubMed: 16735604]
65. Millucci L, Paccagnini E, Ghezzi L, Bernardini G, Braconi D, Laschi M, Consumi M, Spreafico A, Tanganelli P, Lupetti P, Magnani A, Santucci A. Different factors affecting human ANP amyloid aggregation and their implications in congestive heart failure. *PLoS ONE*. 2011; 6:e21870. [PubMed: 21814559]
66. Miklossy J. Emerging roles of pathogens in Alzheimer disease. *Expert Rev Mol Med*. 2011; 13:e30. [PubMed: 21933454]
67. Bu XL, Yao XQ, Jiao SS, Zeng F, Liu YH, Xiang Y, Liang CR, Wang QH, Wang X, Cao HY, Yi X, Deng B, Liu CH, Xu J, Zhang LL, Gao CY, Xu ZQ, Zhang M, Wang L, Tan XL, Xu X, Zhou HD, Wang YJ. A study on the association between infectious burden and Alzheimer's disease. *Eur J Neurol*. 2014
68. Teplov DB. Preparation of amyloid  $\beta$ -protein for structural and functional studies. *Meth Enzymol*. 2006; 413:20–33. [PubMed: 17046389]
69. Bruatto M, Gremmi M, Nardacchione A, Amerio M. Effect of glucose starvation on germ-tube production by *Candida albicans*. *Mycopathologia*. 1993; 123:105–110. [PubMed: 8264767]
70. Stromnes IM, Goverman JM. Active induction of experimental allergic encephalomyelitis. *Nat Protoc*. 2006; 1:1810–1819. [PubMed: 17487163]
71. Miller SD, Karpus WJ. Experimental autoimmune encephalomyelitis in the mouse. *Curr Protoc Immunol*. 2007 Chapter 15, Unit 15.11.
72. Choi SH, Veeraraghavalu K, Lazarov O, Marler S, Ransohoff RM, Ramirez JM, Sisodia SS. Non-cell-autonomous effects of presenilin 1 variants on enrichment-mediated hippocampal progenitor cell proliferation and differentiation. *Neuron*. 2008; 59:568–580. [PubMed: 18760694]
73. Powell JR, Ausubel FM. Models of *Caenorhabditis elegans* infection by bacterial and fungal pathogens. *Methods Mol Biol*. 2008; 415:403–427. [PubMed: 18370168]
74. Henry-Stanley MJ, Garni RM, Wells CL. Adaptation of FUN-1 and Calcofluor white stains to assess the ability of viable and nonviable yeast to adhere to and be internalized by cultured mammalian cells. *Journal of Microbiological Methods*. 2004; 59:289–292. [PubMed: 15369865]

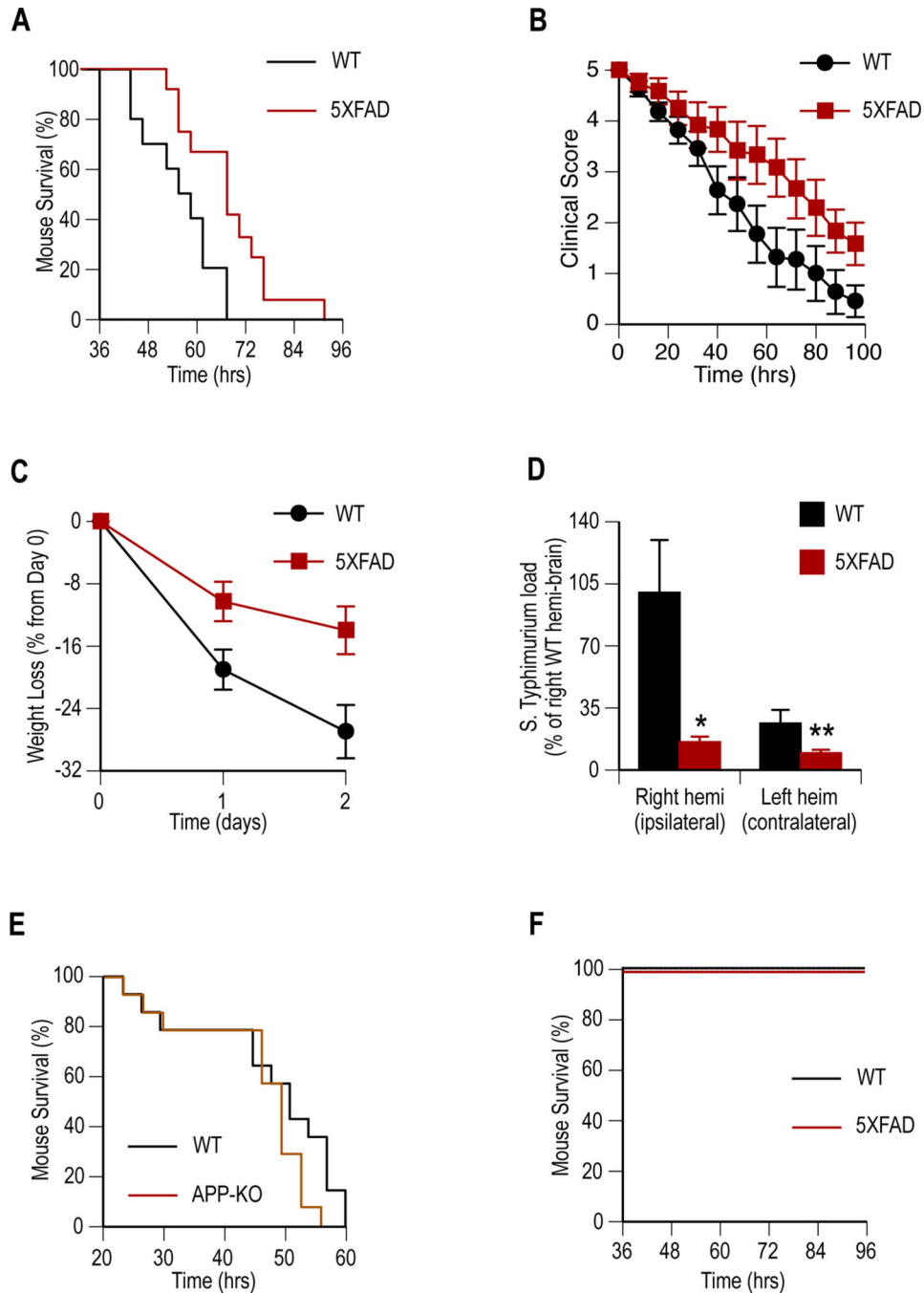


**Fig. 1. A $\beta$  expression protects against *S. Typhimurium* meningitis in genetically modified AD mouse models**

Transgenic (5XFAD) mice expressing human A $\beta$  and mice lacking murine APP (APP-KO) were compared to genetically unmodified littermates (WT) for resistance to *S. Typhimurium* meningitis. One-month old mice received single ipsilateral intracranial injections of *S. Typhimurium* and clinical progression was followed to moribundity. (A to C) Performance of 5XFAD ( $n=12$ ) mice compared to WT ( $n=11$ ) are shown following infection for survival ( $P=0.009$ ) (A), clinical score ( $P<0.0001$ ) (B), percent weight loss ( $P=0.0008$ )



(C). (D) *S. Typhimurium* load 24 hours post-infection in 5XFAD ( $n = 4$ ) and WT ( $n = 4$ ) mouse brain hemisphere homogenates shown as mean CFU  $\pm$  SEM (\* $P = 0.03$  and \*\* $P = 0.04$ ). (E) APP-KO mice ( $n = 15$ ) show a trend ( $P = 0.104$ ) towards reduced survival compared to WT ( $n = 15$ ) littermates following infection. (F) No mortality was observed among control sham-infected WT ( $n = 6$ ) or 5XFAD ( $n = 6$ ) mice injected with heat-killed *S. Typhimurium*. Statistical significance was calculated by Log-rank (Mantel-Cox) test for survival (A, E, and F), linear regression for clinical score and weight (B and C), and statistical means compared by t-test (D). For survival and clinical analysis (A to C) data were pooled from three independent experiments.

Author Manuscript

Author Manuscript

Author Manuscript

Author Manuscript

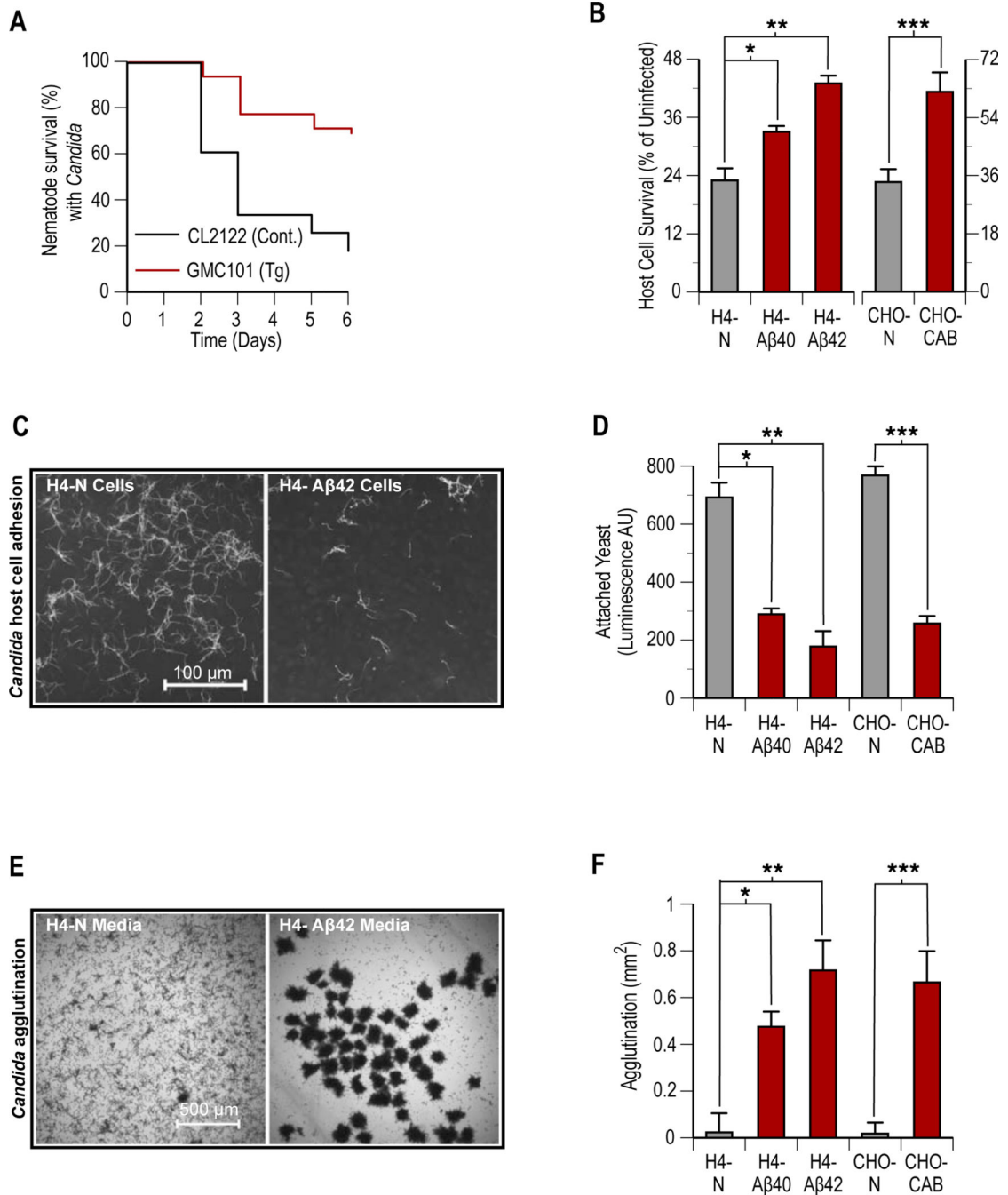


**Fig. 2. Aβ expression in nematodes and cultured cells increases host resistance to infection by *Candida***

Aβ-mediated protection against *C. albicans* (*Candida*) was characterized in *C. elegans* and cultured host cell monolayer mycosis models. Experimental nematodes included control non-Aβ expressing (CL2122) and transgenic human Aβ-expressing (GMC101) strains. Host cell lines included control non-transformed (H4-N and CHO-N) and transformed human Aβ-overexpressing (H4-Aβ40, H4-Aβ42, and CHO-CAB) cells. (A) Survival curves for CL2122 ( $n = 61$ ) and GMC101 ( $n = 57$ ) nematodes following infection with *Candida* ( $P <$

0.00001). **(B)** Viability of non-transformed and transformed host cell monolayers following 36 hours of incubation with *Candida*. Host cell viability was followed by pre-labeling host cell monolayers with BrdU and then comparing wells for an anti-BrdU signal. Signal of infected wells shown as percentage of uninfected control wells (\* $P=0.002$ , \*\* $P=0.001$ , and \*\*\* $P=0.004$ ). **(C)** *Candida* adherence to host cells. Fluorescence micrograph of Calcofluor White stained *Candida* adhering to control **H4-N** or transformed **H4-A $\beta$ 42** host cell monolayers following 2 hours of co-incubation in pre-conditioned culture media. **(D)** Quantitative analysis of *Candida* host cell colonization. Adhering *Candida* were detected using a immunochemical luminescence assay with anti-*Candida* antibodies (\* $P=0.003$ , \*\* $P=0.001$ , and \*\*\* $P=0.004$ ). Well comparisons use arbitrary luminescence units (**AU**). **(E)** Phase contrast micrographs of agglutinated *Candida* following overnight incubation with **H4-N** or **H4-A $\beta$ 42** host cells. **(F)** Quantitative analysis of *Candida* agglutination. Wells were compared for yeast aggregate surface area using image analysis software (\* $P=0.007$ , \*\* $P=0.002$ , and \*\*\* $P=0.009$ ). Bars in panel's (B), (D), and (F) are means of six replicate wells  $\pm$  SEM. Statistical significance was calculated by Log-rank (Mantel-Cox) test for nematode survival (**A**) and statistical mean comparisons by t-test (B, D, and F). Micrographs (C and E) are representative of data from three replicate experiments and multiple discrete image fields (table S1A).

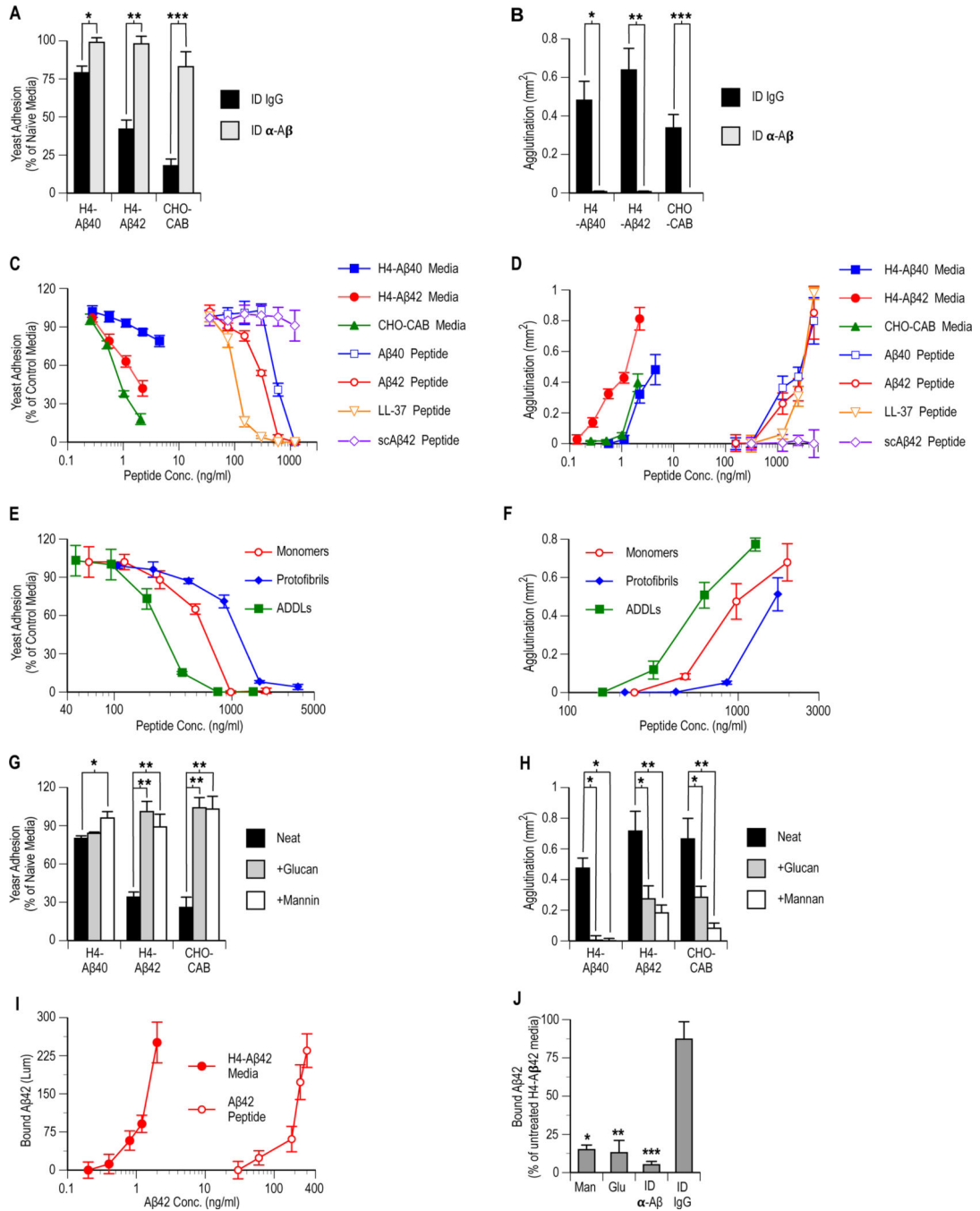


**Fig. 3. Aβ's protective actions in cell culture are mediated by adhesion inhibition and agglutination activities against *Candida***

*C. albicans* adhesion to abiotic surfaces and agglutination in the bulk phase were characterized in the presence of cell-derived or synthetic Aβ. After 36 hours conditioning, host cell free culture media was collected from control non-transformed (H4-N or CHO-N) or transformed Aβ-overexpressing (H4-Aβ40, H4-Aβ42, or CHO-CAB) cultured cells. Aβ-immunodepleted (ID β-Aβ) and control immunodepleted ([ID IgG (immunoglobulin)] media were prepared by incubation with immobilized anti-Aβ or nonspecific antibodies.

Experimental synthetic peptides included A $\beta$  (**A $\beta$ 40** and **A $\beta$ 42**), AMP positive control (**LL-37**), and negative control scrambled A $\beta$ 42 (**scA $\beta$ 42**). (**A** and **B**) Comparison of **ID  $\beta$ -A $\beta$**  and **ID IgG** media's adhesion inhibition (\* $P$  = 0.009, \*\* $P$  = 0.001, and \*\*\* $P$  = 0.004) and agglutination (\* $P$  = 0.001, \*\* $P$  = 0.0005, and \*\*\* $P$  = 0.004) activities. (**C** and **D**) Comparison of anti-*Candida* activities of serially diluted conditioned media and synthetic peptides. (**E** and **F**) Activities of synthetic A $\beta$ 42 monomer, soluble oligomeric amyloid- $\beta$  derived diffusible ligands (**ADDLs**), and protofibril preparations. (**G** and **H**) Conditioned culture media adhesion inhibition (\* $P$  = 0.003 and \*\* $P$  < 0.0003) and agglutinating (\* $P$  < 0.02 and \*\* $P$  < 0.003) source activities alone (**Neat**) or in the presence of soluble yeast wall carbohydrates (+**Glucan** or +**Mannan**). (**I**) Synthetic monomeric A $\beta$ 42 and cell-generated peptide from H4-A $\beta$ 42 cells were compared for *Candida* binding using an A $\beta$ /*Candida* binding ELISA. (**J**) Untreated, immunodepleted, or glucan (**Glu**)- or mannan (**Man**)-spiked H4-A $\beta$ 42 conditioned media were incubated with intact immobilized yeast cells in an A $\beta$ /*Candida* binding ELISA assay (\* $P$  = 0.006, \*\* $P$  = 0.008, and \*\*\* $P$  < 0.004). Synthetic peptide incubations (C to F and I) were performed in H4-A $\beta$ 42 conditioned culture media pre-treated to remove cell-derived A $\beta$  by  $\alpha$ -A $\beta$  immunodepletion. Symbols and bars for (A) to (J) are statistical means of 6 replicate wells  $\pm$  SEM. Statistical significance was by t-test.

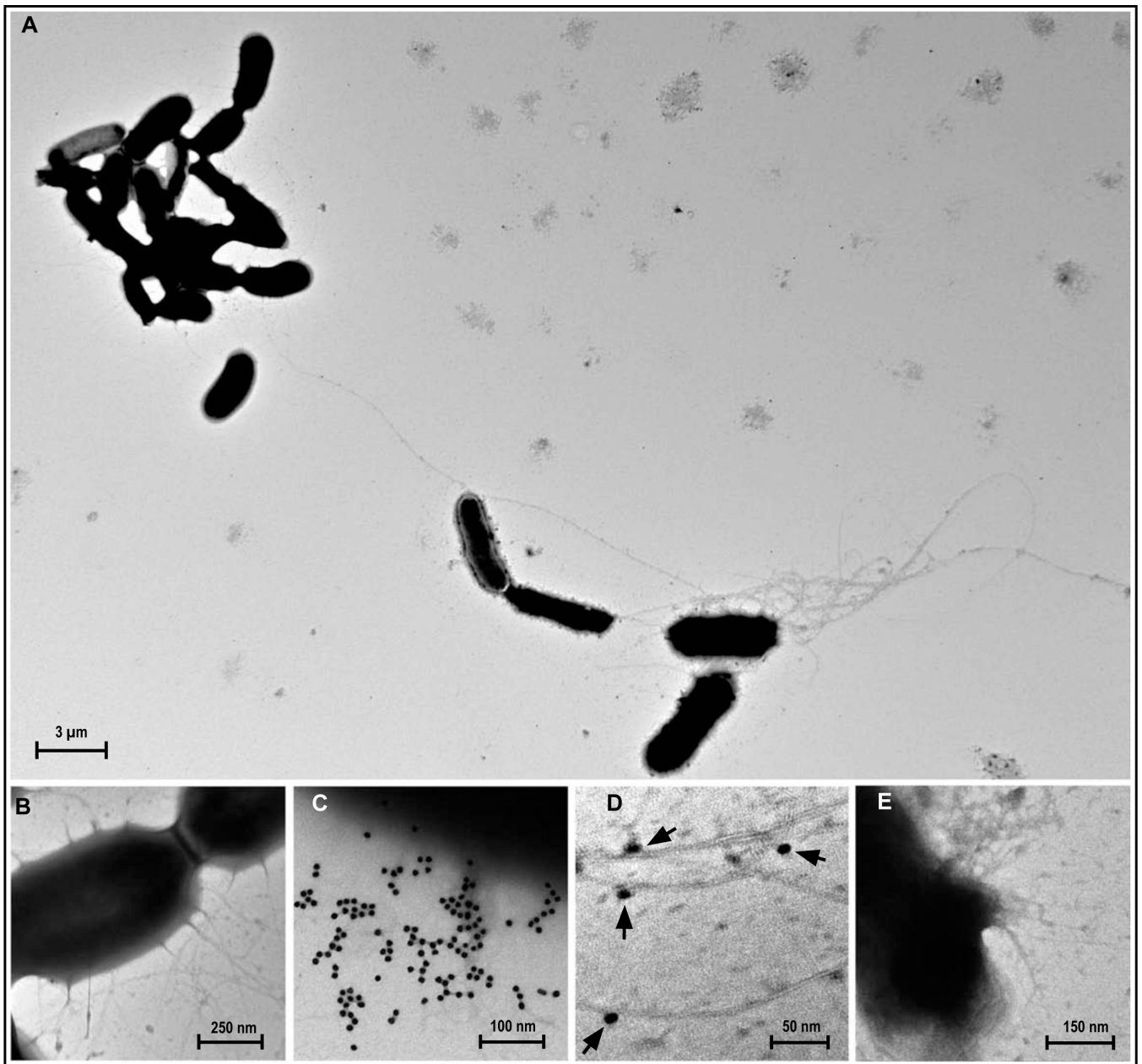


**Fig. 4.  $\beta$ -amyloid fibrils propagate from yeast surfaces and capture *Candida* in H4-A $\beta$ 42 media**  
 Early stage *C. albicans* aggregates harvested from H4-A $\beta$ 42 conditioned media were probed with  $\alpha$ -A $\beta$ -Au nanoparticles and analyzed by TEM. (A) Yeast agglutination is mediated by fibrillar structures. Micrograph shows fibrils binding cells within yeast aggregates and linking *C. albicans* clusters. (B) Fibrillar structures extending from yeast cell surfaces. (C and D)  $\alpha$ -A $\beta$ -Au nanoparticle labeling of short fibrillar structures extending from *C. albicans* surfaces and long fibrils running between yeast clumps. (E) Absorption experiment showing ablated  $\alpha$ -A $\beta$ -Au binding of fibrils extending from yeast in the presence of soluble synthetic A $\beta$  peptide. Data are consistent with specific  $\alpha$ -A $\beta$ -Au labeling of  $\beta$ -amyloid

fibrils. Micrographs are representative of data from three replicate experiments and multiple discrete image fields (table S1A).

Author Manuscript

Author Manuscript

Author Manuscript

Author Manuscript

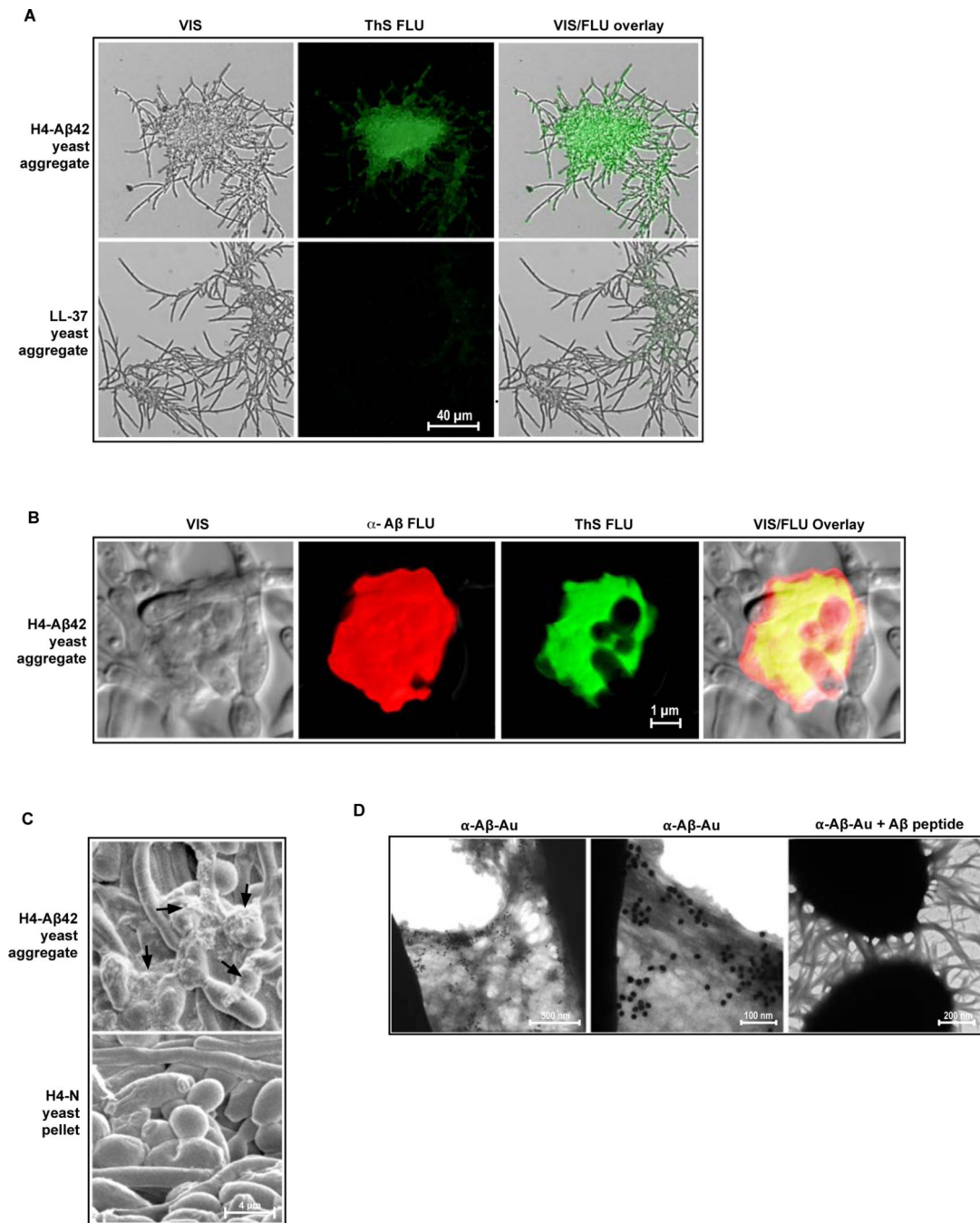


**Fig. 5. *Candida* cells are entrapped by  $\beta$ -amyloid in H4-A $\beta$ 42 culture media**

Following overnight incubation with H4-A $\beta$ 42 media, yeast (*C. albicans*) aggregates were harvested and probed for  $\beta$ -amyloid markers. (A and B) Visible yeast aggregates (VIS), yeast aggregates stained with green-fluorescence Thioflavin S (Thioflavin S FLU), yeast aggregates stained with red-fluorescence anti-A $\beta$  ( $\alpha$ -A $\beta$  FLU); superpositioned images (VIS/FLU overlay). Yeast aggregates generated with the control synthetic LL-37 peptide (A) are negative for Thioflavin S enhanced fluorescence. (B) Yellow denotes co-localization of anti-A $\beta$  and Thioflavin S signals. Co-localization of these signals is the hallmark of  $\beta$ -



amyloid. (C) SEM analysis revealed fibrous material in H4-A $\beta$ 42 yeast aggregates that is absent from control *C. albicans* pellets prepared by centrifugation in H4-N media. (D) H4-A $\beta$ 42 yeast aggregates incubated with immunogold nanoparticles coated with anti-A $\beta$  antibodies ( **$\alpha$ -A $\beta$ -Au**) and analyzed by TEM. First and second panels show labeling of fibrous material by  **$\alpha$ -A $\beta$ -Au**. Third panel shows inhibition of  $\alpha$ -A $\beta$ -Au nanoparticle binding by soluble synthetic A $\beta$  peptide ( **$\alpha$ -A $\beta$ -Au + A $\beta$  peptide**), consistent with specific labeling of  $\beta$ -amyloid. Micrographs are representative of data from two or more replicate experiments and multiple discrete image fields (table S1A).

Author Manuscript

Author Manuscript

Author Manuscript

Author Manuscript

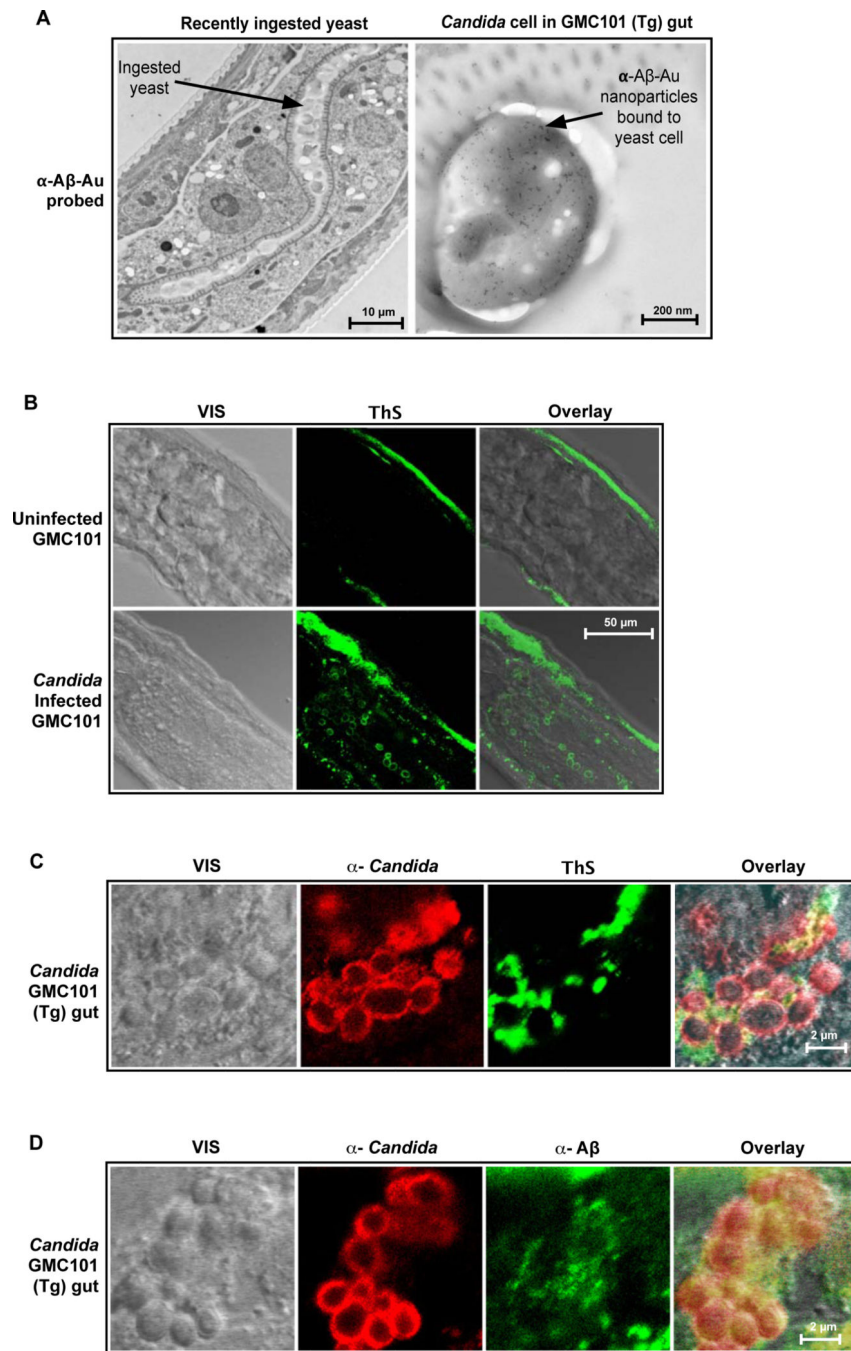


**Fig. 6. Intestinal infection with *Candida* induces A $\beta$  fibrillization in transgenic GMC101 nematode gut**

A $\beta$ 42-expressing GMC101 *C. elegans* were infected with *C. albicans* (*Candida*) and probed for anti-A $\beta$  immunoreactivity and  $\beta$ -amyloid markers using TEM and confocal microscopy CFM. (A) Micrograph shows positive labeling of yeast cell surface in GMC101 worm gut by immunogold nanoparticles coated with anti-A $\beta$  antibodies ( $\alpha$ -A $\beta$ -Au) two hours following *Candida* ingestion. (B and D) Figures show visible (VIS) and fluorescence signals from freeze fracture nematode sections with advanced *Candida* infections. Figure B compares

uninfected and infected worms. Figures C and D show Thioflavin S and anti-A $\beta$  staining for gut yeast aggregates. Signals include anti-*Candida* immunoreactivity  $\alpha$ -*Candida*), Thioflavin S enhanced fluorescence (**ThS**), anti-A $\beta$  immunoreactivity ( **$\alpha$ -A $\beta$** ), and superpositioned (**Overlay**) signals . Yellow denotes signal co-localization. Uninfected and infected CL2122 nematode controls were negative for anti-A $\beta$  immunoreactivity and enhanced Thioflavin S fluorescence (figs. 2S and S8). Micrographs are representative of data from three or more replicate experiments and multiple discrete image fields (Table S1B).

Author Manuscript

Author Manuscript

Author Manuscript

Author Manuscript

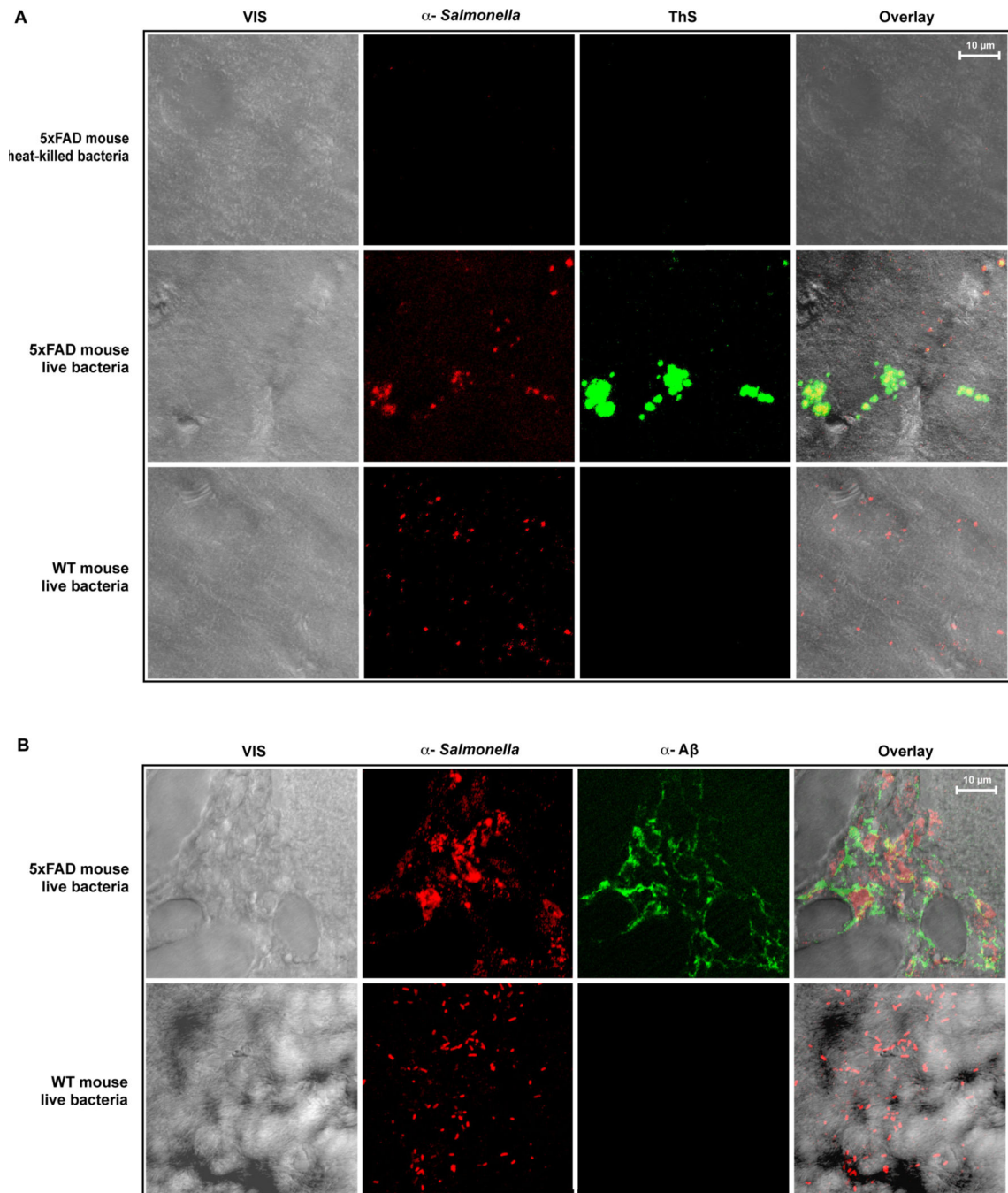


**Fig. 7. Infection-induced  $\beta$ -amyloid deposits co-localize with invading *S. Typhimurium* cells in 5XFAD mouse brain**

Four-week-old wildtype (WT) mice or transgenic 5XFAD animals expressing high levels of human A $\beta$  were injected intracerebrally with viable *S. Typhimurium* bacteria. Mice were also injected with heat-treated *S. Typhimurium* cell debris as a negative control for the injection procedure. (A and B) Mouse brain sections were prepared 24 (A) or 48 hours (B) after infection. Signals shown include visible (VIS), anti-*Salmonella* immunoreactivity ( $\alpha$ -*Salmonella*), enhanced Thioflavin S fluorescence (ThS) or anti-A $\beta$  immunoreactivity ( $\alpha$ -

**A $\beta$** ), and superpositioned (**Overlay**) signals. Panels are representative images of multiple images captured as z-sections using confocal fluorescence microscopy . Yellow denotes signal co-localization. (Z-series projections showing  $\beta$ -amyloid surrounding and entrapping bacteria colonies in a rotating 3-dimension section of 5XFAD mouse brain are also included in video S1). Micrographs are representative of data from three replicate experiments and multiple discrete image fields (table S1C).

Author Manuscript

Author Manuscript

Author Manuscript

Author Manuscript